SSRG International Journal of Civil Engineering
ISSN: 2348-8352/ https://doi.org/10.14445/23488352/IJCE-V13I5P119

Volume 13 Issue 5, 284-308, May 2026

Original Article

Assessment of Groundwater Potential and Quality in Erode Taluk through Electrical Resistivity Sounding, Water Quality Index, and Multivariate Statistical Analysis

Darshan Mehta[1*], Ravi Ande[2], Utkarsh Nigam[3], Chaitali Bhavsar[3], Akshay Rathod[4], Prashant Sunagar[5]

[1]*Department of Civil Engineering, Dr. S. & S. S. Ghandhy Government Engineering College, Surat, Gujarat, India.*
[2]*Lady Irwin College, University of Delhi, New Delhi, India.*
[3]*Department of Civil Engineering, L. D. College of Engineering, Ahmedabad, Gujarat, India.*
[4]*Department of Civil Engineering, Gujarat Technological University - Institute of Technology and Research, Mehsana, India.*
[5]*Department of Civil Engineering, Sandip Institute of Technology and Research, Nashik, Maharashtra, India.*

[*]*Corresponding Author : ap_darshan_mehta@gtu.edu.in*

Received: 10 February 2026 Revised: 25 March 2026 Accepted: 29 April 2026 Published: 29 May 2026

Abstract - *Groundwater samples collected from open wells and bore wells in Erode Taluk, Erode District, South India, were analyzed to evaluate the spatio-temporal variations in hydrochemistry and overall groundwater quality. A total of 103 groundwater samples were obtained over an eleven-year period (January 2014 to December 2024) from sampling locations situated along the Cauvery River, approximately 100 km east of Coimbatore. The samples were examined for a comprehensive suite of physicochemical parameters, including pH, EC, TDS, TH, major cations (Ca^{2+}, Mg^{2+}, Na^{+}, K^{+}), major anions (HCO_3^{-}, CO_3^{2-}, Cl^{-}, SO_4^{2-}, NO_3^{-}, F^{-}), and trace metals (Fe, Mn, As, Cd, Cr, Cu, Zn, Pb, and Hg). Premonsoon pH values indicated groundwater conditions ranging from slightly acidic to alkaline. The dominant ionic abundance followed the order $Na^{+} > Ca^{2+} > Mg^{2+} > K^{+}$ and $HCO_3^{-} > Cl^{-} > SO_4^{2-} > CO_3^{2-}$, reflecting the prevailing geochemical processes within the aquifer system. Water Quality Index (WQI) analysis demonstrated that most groundwater samples fell within the "Excellent to Good" category. Regression analysis between WQI and selected parameters yielded strong correlations, with coefficients of determination (R^2) of 0.82 for the premonsoon and 0.92 for the postmonsoon seasons, indicating pronounced seasonal influences on groundwater quality. Rainfall analysis revealed that the Northeast (NE) monsoon contributes the highest share of annual rainfall (49.39%), followed by the Southwest (SW) monsoon (28.54%) and the premonsoon period (21.41%), while the postmonsoon season accounts for less than 0.65%. The average NE monsoon rainfall (373.55 mm) was significantly higher than that of the SW monsoon (222.37 mm). Ten-year rainfall trends showed higher precipitation during 2014–2016, followed by a declining trend from 2018 to 2024. Seasonal groundwater level analysis indicated variations ranging from 3.39–7.76 m during the postmonsoon, 3.85–7.61 m during the premonsoon, 4.48–7.07 m during the SW monsoon, and 3.50–6.24 m during the NE monsoon. The annual groundwater level fluctuation ranged from a minimum of 4.14 m in 2022 to a maximum of 7.04 m in 2015. In addition, multivariate statistical methods, including factor analysis and cluster analysis, were employed to support the interpretation of hydrochemical processes and the evolution of groundwater quality within the study area.*

Keywords - *Groundwater Quality, Hydrochemistry, pH, Regression Analysis, Seasonal Variation, Water Quality Index.*

1. Introduction

The most valuable resource that is necessary for all living things to exist is water. India is very concerned about the growing demand for clean water on the one hand, and the declining supply and declining quality on the other. The primary determinants of groundwater quality are the aquifer formation's physical and chemical characteristics. Therefore, a comprehensive understanding of the geochemical mechanisms that drive groundwater chemistry is necessary to understand and address groundwater-related concerns. The physical, chemical, and biological properties of water are the main factors that define its quality. The study of the chemical makeup of the Earth, including rocks and minerals, as well as the mechanisms governing their distribution, is the main emphasis of geochemistry. Chemistry, on the other hand, deals with the composition, properties, and reactions of substances at the atomic and molecular levels. Approximately 71% of the Earth's surface is covered by

water, highlighting its critical importance for environmental and human systems (Adnan M. Aish 2013). All known life forms depend on it, and because meteoric precipitation replenishes it every year, it is a renewable resource. Seas and oceans contain 96.5% of the world's water, glaciers contain 1.7%, Groundwater and the ice caps of Greenland and Antarctica contain 1.7%, other large bodies of water contain a very small portion, and clouds, precipitation, and vapour make up the remaining 0.001% of the atmosphere (Aglos Papaioannou &Athina Mavridou, 2000).

Large concentrations of total dissolved solids (more than 1500 mg/l) render them unfit for agricultural and drinking purposes. The study of surface and Groundwater's chemical characteristics in connection to local and regional geology is known as hydrochemistry. Surface water is more vulnerable to pollution than Groundwater because it is simpler to access for the discharge of wastes (Aldrian, E.,& Setiawandjamil, Y 2008). Because of their proximity to urban areas, the freshwater bodies in this case are susceptible to rapid deterioration processes caused by an increase in pollution caused by humans. In India, about 30% of urban and 90% of rural residents depend on Groundwater for agricultural and home uses (Anandakumar, S,.2007). Additionally, it accounts for around 60% of the country's irrigation potential. Due to regional local differences in geology and temperature, as well as spatiotemporal variance in rainfall, Groundwater is distributed unevenly throughout the country (Subramani, T., & Elango, L., 2007).

Studies using GIS tools have verified that factors including the length, slope, and watershed boundary are crucial for assessing Groundwater. Each theme's many units are ranked from 1 to 4 according to a knowledge-based hierarchy, and their importance is evaluated by their groundwater potential (Aditya, M 2009). The supply of high-quality water for drinking and agriculture is an issue because of the fast expansion of industry, urbanization, and the resulting threat of water contamination. By digging observation wells, researchers have been able to analyze rainfall variations, analyze groundwater level fluctuations, and evaluate the physicochemical properties of Groundwater. Water level measurements and water sample analysis have been used to routinely monitor the observation wells (Benyahya, L, & Caissie, D,2007).

The United States, Bangladesh, China, India, Iran, Pakistan, and other nations consume 80% of the world's Groundwater; the world's largest groundwater irrigator is India. Groundwater development has played a major role in reducing poverty in rural areas. This is because, compared to extensive surface water irrigation projects, groundwater irrigation often discriminates less against people experiencing poverty (Basarin, B., and Lukić, T.,2016). Farmers and small groups can swiftly develop Groundwater since it is readily available, dependable, and adaptable in terms of time and location. Additionally, Groundwater offers lower evaporation losses than surface dams or canals from the standpoint of water management. Compared to traditional canal irrigation systems, which were mostly developed by the colonial government in the late 1800s, Groundwater is utilized to irrigate a greater region of India (Bhat, B., & Parveen, S., 2018).

1.1. Previous Studies of Research

In Erode Taluk, Groundwater is the primary resource for supplying the population's drinking and irrigation needs because surface water is insufficient to meet demand. Consequently, a thorough investigation has been conducted to identify the groundwater potential zones and evaluate the Groundwater's appropriateness for irrigation and drinking (Blaszczak, J. R., & Koenig, L. E., 2023). Using geophysical surveys conducted at several points throughout the research area, an effort has been made to comprehend the demarcation of the Groundwater potential zone. Utilising GIS and ANFIS approaches, the regional variation of groundwater quality and its appropriateness for irrigation and consumption has been examined (Cai, H., and Piccolroaz, S.,2018).

1.2. Objectives of Research

With these objectives in view, the present study aims to generate and integrate relevant datasets to comprehensively evaluate the groundwater resource potential and quality in Erode Taluk, Tamil Nadu, India, using appropriate scientific methodologies. Using GIS tools, create a variety of themed maps pertaining to studies on groundwater quality. Identify the groundwater prospective zones and comprehend variations in rainfall and groundwater level. To use a GIS to plot the groundwater geochemistry's seasonal and regional variations (Choi, S. Y., & Seo, I. W., 2018).

1.3. Scope of Future Research

There is room for more research, according to the investigation: the study can be expanded to include additional environmental pollutants like soil and air. Installation of several manufactured recharge structures for the areas where groundwater potential is weak. It is possible to conduct research on how untreated industrial effluent and municipal sewage affect the quality of Groundwater. Research on the socioeconomic effects of water budgeting for areas that are polluted suggests that remediation methods may be recommended (Chen, G., & Fang, X.,2015).

1.4. Research Gap

In India, both rural and urban residents primarily obtain their drinking water from Groundwater. Drinking water is scarce, particularly during the summer, due to excessive groundwater extraction to satisfy home, industrial, and agricultural demands. As a result, research on groundwater quantity and quality, one of the most crucial aspects of groundwater management, has received particular attention. Since surface water is insufficient to support the population's

drinking and irrigation needs in Erode Taluk, Groundwater is the primary supply. To identify groundwater potential zones and assess whether Groundwater is suitable for irrigation and drinking, a thorough examination was conducted. In this work, geophysical surveys at several places within the study region have been used to try to understand the demarcation of the Groundwater potential zone. To use GIS tools to create a variety of themed maps pertaining to groundwater quality investigations. To comprehend the fluctuations in groundwater levels and rainfall. To identify potential groundwater zones using geophysical survey methods. To use GIS to plot the seasonal and spatial fluctuation in groundwater geochemistry.

1.5. Review of Literature

The thematic mapping of Groundwater was performed using datasets collected from the Geological Survey of India, Survey of India (1981), and Landsat Thematic Mapper imagery. Each of the following layers was created through the digital interpretation of 30 m resolution imagery: geology, soil, drainage, LULC, geomorphology, lineament, drainage density, and lineament density.

The spatial distribution of the major ions within the subsurface was determined relative to World Health Organization guidelines using ArcGIS.

Inverse Distance Weighting (IDW) was utilized to determine the spatial distribution of the different water quality parameters.

The integration of each of the thematic maps allowed for the delineation of the zones with the best groundwater quality.

1.5.1. Gaps in Literature

The robustness of the models was ensured through calibration and validation to allow for the reliable prediction of groundwater quality. A total of 103 groundwater samples were collected from the study area during both pre- and post-monsoon periods in 2024 and analyzed for various physicochemical parameters. Geoelectrical methods were utilized for the subsurface investigation of the study area.

Due to the cost-efficient nature of these methods, they were employed to determine the subsurface resistivity of the area. Geo-electrical surveys measure the Voltage (V) and current (I) that are present in the subsurface to calculate the resistivity of the ground. Schlumberger, Wenner, Dipole–Dipole, and Two-Electrode arrays are some of the most common geoelectrical array configurations used in subsurface investigations (Table 1).

Table 1. Review of literature

S. No	Reference	Year	Research Topic
1	Aditya, M	2009	Evaluation of Groundwater in the Gadilam Basin using isotope and hydrogeochemical data
2	Adnan M. Aish	2013	Ground water quality maps of Paravanar river sub basin, Cuddalore district,
3	Paul, AL	2000	Shallow aquifer zone delineation in the northwest of Bhuvanagiri, Chidambaram Taluk, Cuddalore District,
4	Al-Zubaidi, H. A.	2023	Groundwater chemical characterisation in the eastern coastal region of Tamil Nadu's Cuddalore district.
5	Ouarda, T. B., & Bobée, B.	2007	Assessment of Groundwater Quality Spatial Variability in the Paravanar River Sub-Basin, Cuddalore District, Tamil Nadu
6	Carter, A. M., & Cohe M. J.	2023	Evaluation of Depth-Wise Variations in Hydrogeology and Hydrogeochemistry of Groundwater in a Coastal Aquifer at Annamalai Nagar,
7	Schmidmeier, J., & Barth, J. A.	2022	A case study from the Cuddalore area in Tamil Nadu, south India, on the hydrogeochemical features of coastal aquifers
8	Hood, J. M., & Freitag, T. E.	2016	Physicochemical examination of groundwater samples in the Cuddalore district of Tamil Nadu, India, close to an industrial location

2. Materials and Methods

2.1. The Study Area

Erode Taluk, a special grade municipal town in the Erode Region, is on the banks of the River Cauvery, 100 km east of Coimbatore. It is located between longitudes 77° 36' 39.857 and 77° 55' 46.25 E and latitudes 11° 01' 33.067 and 11° 27' 42.163 N. Figure 1 depicts Erode Taluk, which is 752.61 km2 in total size (Caissie, D., & Luce, C. H., 2017). The seven taluks that make up the Erode Region are further divided into twenty blocks. Erode Taluk is made up of three blocks: Kodumudi, Modakurichi, and Erode. March marks the start of the hot season, which lasts until May when it peaks at 40°C. The four distinct seasons of winter, the hot weather period, the Southwest monsoon, and the Northeast monsoon all have an impact on the region's average annual rainfall of 660.10 mm (Daneshi, J., Naserin, A.,2023). Red calcareous soil (40.43%) and red non-calcareous soil (47.02%) make up most of the research area, with alluvial soil (12.55%) occupying the smaller sections. In the study area, 852 mm of precipitation falls on average each year. The study region is covered with gneissic rock in terms of geology, as shown in Figure 1 (Dordoni, M., and Seewald, M.,2022).

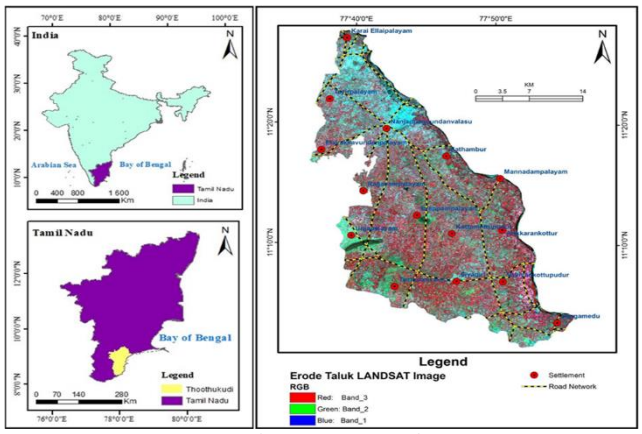

Fig. 1 Location of the study area of Erode Taluk

2.2. Hydro Geomorphology

The occurrence and movement of Groundwater can be directly influenced by structural features, drainage characteristics, and the mapping of different landforms. Finding appropriate groundwater zones is made easier by the landforms in the satellite photos. Below are definitions and descriptions of the several geomorphologic units that were chosen for interpretation using false colour composites, which were conducted on groundwater potential throughout India (Demars, B. O., & Gíslason, G. M.,2016). Groundwater possibilities are good in alluvial plains and valley fills.

High porosity and permeability are two characteristics of the weathered material and thick alluvium that make up valley fills. These characteristics are grouped according to the probability of the presence of Groundwater, and many of them are favourable for the presence of Groundwater. The pediplans valley floor comprises 14.45 km2 of land that is dispersed in all directions. The canal command areas and buried pediplans are classified as being good to moderate in relation to the availability of Groundwater. However, the ridge and inselberg complexes contain zones that are classified as being moderate to poor zones in relation to Groundwater favourable values (Eiden, G., 2008). The units that make up the pediplans, specifically the valley floor and shallow floodplain, are considered to be the most favourable for Groundwater – they contain very good to good zones for Groundwater as depicted in Figure 2(a), 2(b). A discussion of the hydrogeomorphology and drainage density of the land is a valid and effective means of discussing the geology of the study area (Golmohammadi, G., & Rudra, R.,2017). Such discussions of these elements avoid redundancy within the study report and allow for a more detailed analysis of the geological elements of the area. Through examining each of these elements, researchers can gain a more cohesive understanding of how the landscape and hydrology of the area are respective elements of each other (Gupta, H. V., & Sorooshian, S.,1999).

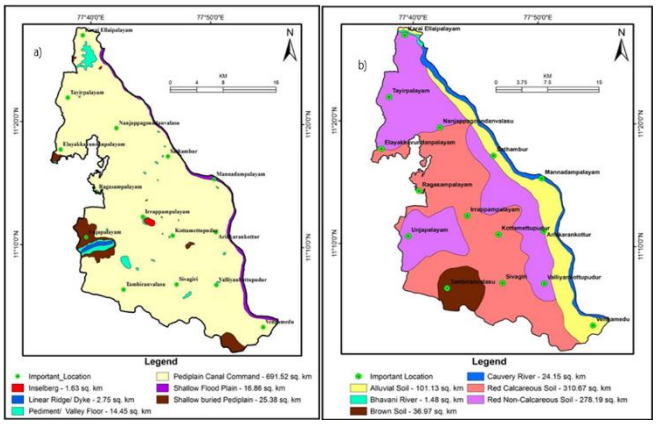

Fig. 2 Hydro geomorphology of red calcareous and red non-calcareous soil (a) premonsoon, and (b) Postmonsoon.

2.3. Drainage Density of Erode Taluk

Drainage patterns are often indicative of the tectonic history of the region and accurately represent the structural features of the region that is buried beneath the overlying surface features. Six of the most prevalent drainage patterns are represented by various types of bedrock and landforms. The dendritic drainage pattern is prevalent in regions that have similar types of bed rocks, such as granite or sedimentary rocks that lie in a flat direction (Hall Jr, R. O., & Yackulic, C. B.,2015). The rectangular drainage system is essentially a dendritic pattern that has been altered by the structural bedrock content such that the tributaries meet at right angles. A massive sandstone that lies flat and has a well-developed joint system is visible. There is a region of folded sedimentary rocks where the trellis drainage is located at right angles (Huryn, A. D., and Benstead, J. P.,2014). The uppermost portion of the research area was where the

clustered drainages were observed. Dentritic and sub-dentritic patterns can be seen on the drainage map, and certain areas exhibit parallel drainage. As seen in Figures 3(a) and 3(b), the majority of the study area exhibits dendritic and subdendritic drainage patterns. Unconfined aquifers contain the research area's Groundwater. The aquifers' condition and slope determine the water level at premonsoon and Post – Monsoon period (Figure 3(a), 3(b)) (Helms, D., 1992).

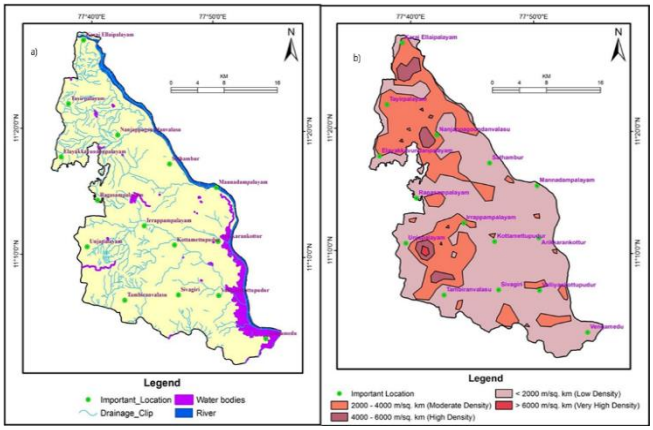

Fig. 3 Drainage density map of the Erode Taluk, (a) premonsoon, and (b) postmonsoon.

2.4. Data Collection and Preparation

Six rain gauge stations within the study area provided rainfall data during a ten-year period (2014–2024). A variety of government agencies provided additional datasets, such as satellite images, rainfall intensity, groundwater levels, and groundwater quality data. Four topographical sheets at a scale of 1:50,000 from the Survey of India (SOI) were used to create the research area's base map. For this reason, the topo sheet numbers 58E/11, 58E/12, 58E/15, and 58E/16 were utilised. Additionally, the Public Works Department (PWD) provided monthly groundwater level data for examinations from January 2014 to December 2024. (Himanshu, S.K., & Pandey, A.,2019). In Erode Taluk, Tamil Nadu, 103 well distinct locations provided groundwater samples, which were chosen at random, a rainfall study flow chart of pre and post-monsoon, NE&SW Monsoon (Figure 4). The American Public Health Association procedure is followed for sampling. Using a water sampler, groundwater samples were taken from open wells 30 cm below the water level. Either an electric motor or a hand pump was used to gather the samples from tube wells (Johnson, A.M., & Truax, D.D.,2002). Before being taken to the field, the samples were rinsed with double-distilled water and placed in premium plastic bottles with a two-liter capacity. After filling the bottles with the samples, the bottles were rinsed with the corresponding well water samples to gather all of the samples (Kalcic, M. M., & Chaubey, I.,2015). Before undergoing physical and chemical examination, the samples are kept in an icebox, brought to the lab within six hours, and refrigerated at 4 °C for major ion measurement.

2.4.1. Temporal Assessment

Groundwater samples taken in 2012 during the premonsoon and postmonsoon seasons were examined for trace elements. The World Health Organization's standards were compared with the analytical data to determine whether the Groundwater was safe to drink. The following is the order of main ion abundance in Groundwater: Na+ > Ca2+ > Mg2+ > K+ = HCO3 > Cl > SO4 2 > NO3 > CO3 2. According to the spatial distribution map, the "Good" category of Groundwater is 495 km^2 and 295.06 km^2 before and after the monsoon season, respectively. As a result of anthropogenic activities, an area of over 200 km2 was moving to the next worst category

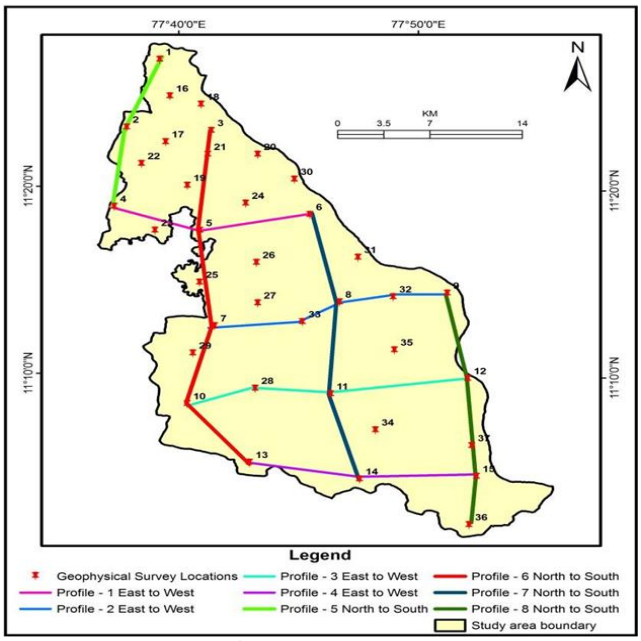

Fig. 4 Location of monitoring samples at Erode Taluk

3. Hydro Geophysical Electrical Sounding Survey

A Schlumberger Vertical Electrical Soundings (VES) survey was conducted. With a maximum electrode separation of 150 meters, the VES investigation was carried out at 37 locations. Figure 5. provides a comprehensive geophysics technique. The poll was conducted at a uniform distance (Legates, D. R., 1999)—specific resistance of a material. Ohm's law provides it in equation (1).

$$\rho = RA/L \quad (1)$$

where ρ = Resistivity and

R is the resistance provided by the cross-sectional area (A) and length (L).

Electrical resistivity methods estimate the electrical resistance. Equation (2) provides the formation's resistivity (Luan, X.,&Wu, P., 2018)

$$\rho = K \times (\Delta v \div I) \quad (2)$$

The electrode arrangement's geometric factor, or K, is calculated using equation (3).

$$K = ((AB/2)^2 - (MN/2)^2) / MN \times \pi \quad (3)$$

Methodology Flaws

The region's average seasonal rainfall is shown by the average rainfall during the premonsoon, postmonsoon, South West, and North East monsoon seasons. Ten years of rainfall data (2004–2024) from six rainfall stations (Erode, Perundurai, Chennimalai, Bhavani, Mettunasuvanpalayam, and Ammapettai) were used to determine the average annual rainfall for the Erode area. For the Erode taluk, an analysis of the rainfall intensity, ERS, and WQI throughout the area according to each of the months of the year was performed. Geological formations in the area have significant variation in their resistivity within and between each formation. Each of these variables impacts the resistivity of the formation in different ways. The temperature of the subterranean area impacts the resistivity of the formation. The amount of water within the aquifer impacts the formation of that area. Finally, the formation, density, and porosity of the aquifer materials determine the amount of water that can be contained within that area.

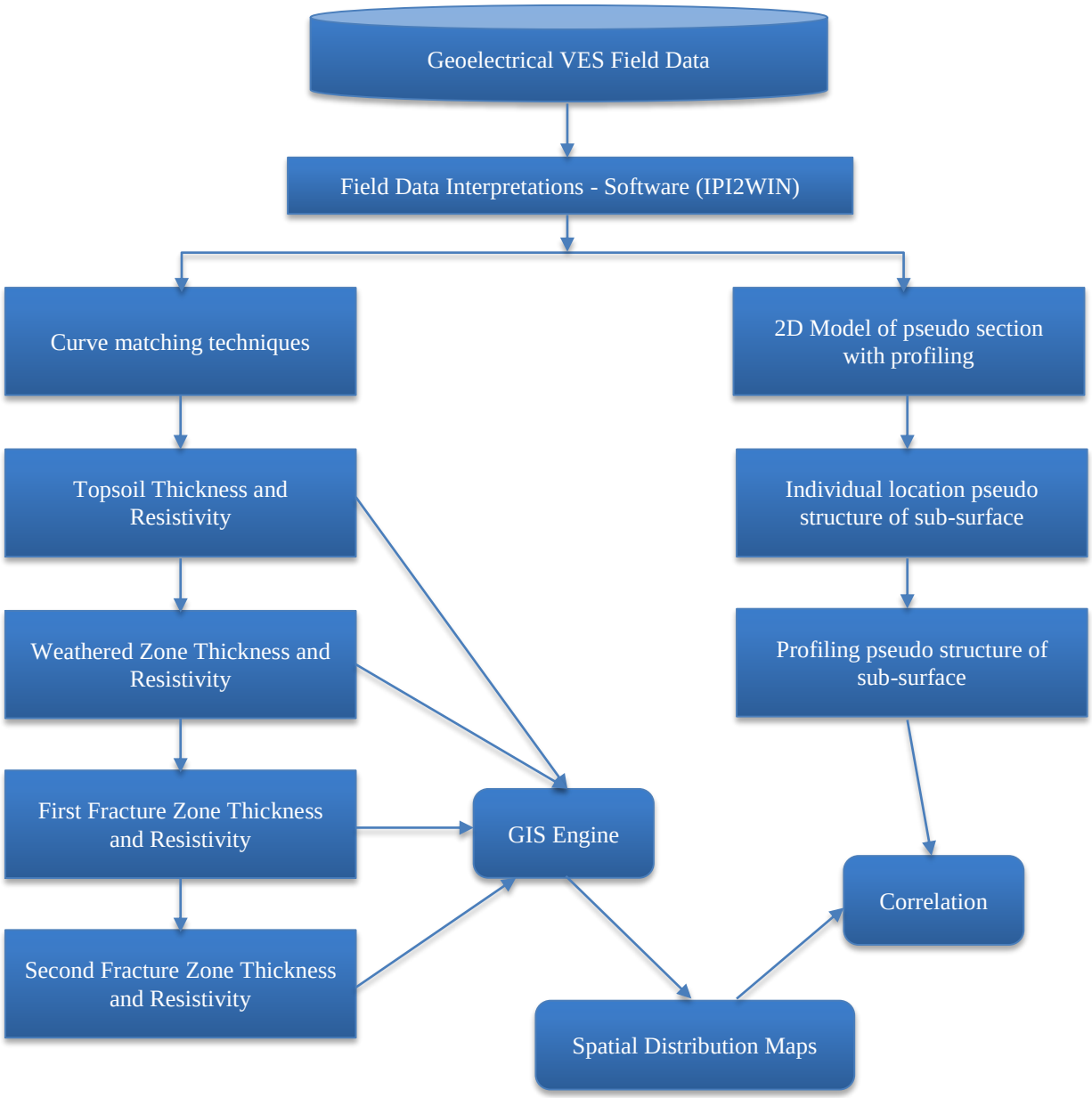

Fig. 5 Geophysical electrical sounding survey flow chart

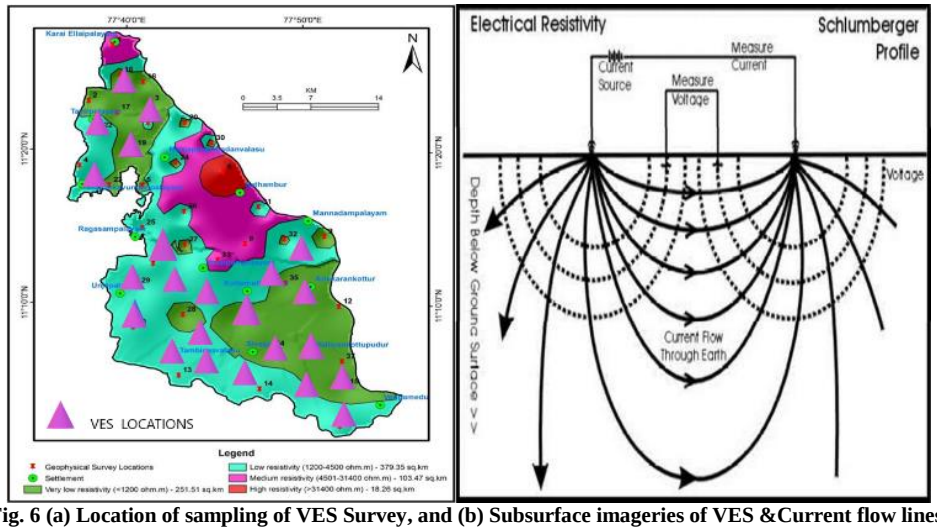

Fig. 6 (a) Location of sampling of VES Survey, and (b) Subsurface imageries of VES &Current flow lines.

Archaean crystalline formations predominate in the study area, with isolated instances of Quaternary valley-fill deposits. Investigation of groundwater conditions in this region is essential due to the acute scarcity of aquifer resources. The Schlumberger resistivity method operates on the principle of contrasting physical properties between subsurface layers and the surrounding medium. In hard rock terrains, fractures may extend to considerable depths, often up to several hundred meters. When these fractures are saturated with Groundwater, they exhibit relatively low resistivity compared to the surrounding compact rocks, thereby providing a clear contrast (Kalcic, M. M., & Chaubey, I., 2015). Resistivity values are influenced by parameters such as porosity, moisture content, degree of mineralization, and lithological characteristics. Accordingly, geophysical investigations aim to establish relationships between resistivity and aquifer hydraulic properties.

In the present study, resistivity data from 37 VES locations were interpreted using curve matching techniques with IPI2WIN software (Kassem & Raheem, 2019). The analysis reveals that the AK-type curve ($q_1 < q_2 < q_3 < q_4$) is the most dominant, covering approximately 27.03% of the study area. This is followed by KH-type curves ($q_1 < q_2 > q_3 < q_4$) accounting for 16.22%, AA-type curves ($q_1 < q_2 < q_3 < q_4$) covering 8.11%, and HK-type curves ($q_1 > q_2 < q_3 > q_4$) representing 5.41%. Additionally, KQ-type and HA-type curves ($q_1 > q_2 < q_3 > q_4$ and $q_1 < q_2 > q_3 > q_4$) together constitute about 2.70% of the area. Notably, the presence of Q-type curves is considered indicative of favorable groundwater potential zones, highlighting areas suitable for groundwater exploration and development (Legates, D. R., and McCabe, G. J.,1999). Table 2 shows the interpretation of geophysical data.

3.1. Profile Cross-Section of the Resistivity Survey

The 2D resistivity pseudo-section represents subsurface conditions along the north–south direction of the study area. This profile covers locations such as Sircar Peria Agraharam, Muthampalayam, Avalpoondurai, Arasalur, and Kongudayanpalayam. Among these, Kongudayanpalayam lies in the lower part of the study area, Avalpoondurai and Arasalur occupy the central region, while Sircar Peria Agraharam and Muthampalayam are situated in the elevated portion. As illustrated in Figure 7, the profile traverses the study area along a north–south alignment (Luan & Wu, 2018). The interpretation of the 2D resistivity section indicates that the Muthampalayam (VES–7) location represents a zone with good groundwater potential. Another electrical resistivity profile (Profile 7) situated in the central part of the study area covers the regions of Punjai Lakkapuram, Modakurichi, Kagan, and Anjur. This profile also extends in the north–south direction, as shown in Figure 7 (Malunjkar & Shinde, 2013). The 2D resistivity section for this profile suggests that the Punjai Lakkapuram VES location exhibits favorable groundwater potential (Mamo, K. H. M., & Jain, M. K., 2013).

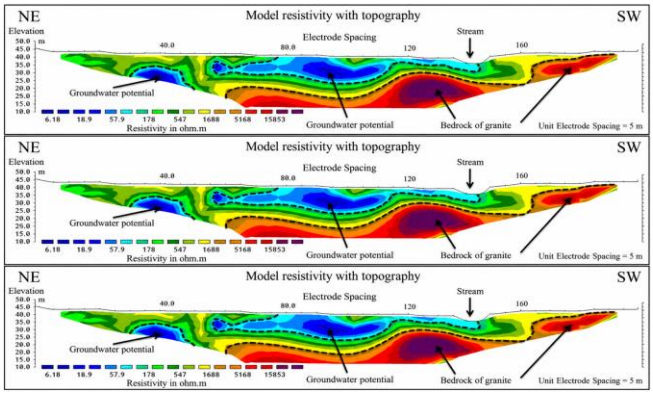

Fig. 7 Pseudo-section in 2D inverse model NE-SW Direction

3.2. Fracture Zone of the Resistivity Layer

The subsurface was delineated into four main zones, including the first and second fractured zones. In some

locations, four-layer resistivity curves were identified, suggesting the presence of a transitional semi-weathered zone between the weathered and fractured layers (Ngo & Binh, 2015). The spatial distribution map of topsoil thickness (Figure 8) indicates zones of extremely high and high thickness, covering approximately 63.36 km² and 323.67 km², with thicknesses exceeding 2.5 m and ranging between 1.71 m and 2.5 m, respectively. These areas, due to their greater thickness, are considered favorable for artificial recharge. In contrast, the remaining regions fall under moderate to low thickness categories and are less suitable for the development of artificial recharge systems (Noori & Kalin, 2016).

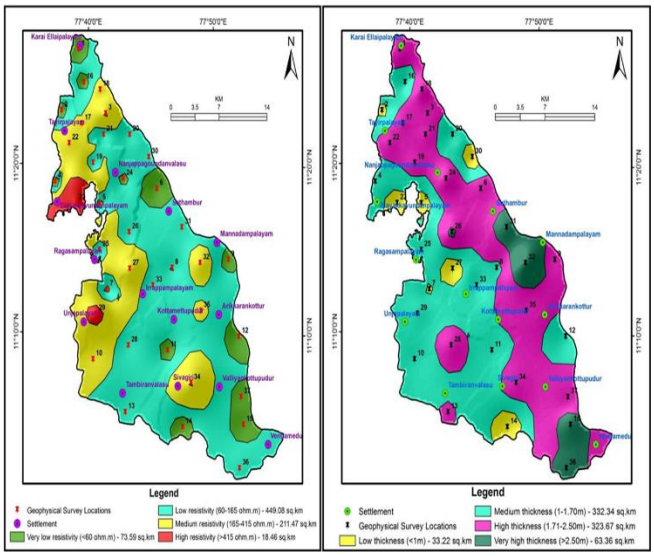

Fig. 8 (a) Spatial variation of topsoil resistivity, and (b) Spatial variation of topsoil thickness.

3.3. Weathered Zone Resistivity and Thickness

The thickness of the weathered zone, along with its minimum and maximum resistivity values, was evaluated using Vertical Electrical Sounding (VES) data. At Karai Elaipalayam (VES–1), the weathered zone extends to a depth of 35.9 m, where relatively high resistivity values indicate the presence of compact rock formations. In contrast, the lowest resistivity value of 10.2 Ω·m was recorded at Avalpoondurai (VES–7) at a shallow depth of 1.04 m. Field observations further confirm the occurrence of hard and compact rock at this depth in nearby open wells, which results in limited groundwater yield in the area. Generally, low resistivity values are associated with water-bearing formations (Shrestha, 2015). The study reveals considerable spatial variation in both resistivity and thickness across the area. Zones with low resistivity (around 10.2 Ohm-m) at shallow depths indicate favorable groundwater potential, while areas with greater weathered zone thickness also support higher groundwater storage (Oluwatosin & Adeyolanu, 2006). Based on the geophysical data, a spatial distribution map of weathered zone resistivity was prepared (Figure 9). The resistivity values were classified into four categories: very low, low, moderate, and high. Among these categories, areas exhibiting very low and low resistivity values are generally associated with favorable groundwater potential zones (Osypov & Osadcha, 2018). These zones cover approximately 61.71 km² and 520.86 km², respectively, making them the most suitable for groundwater development. Additionally, a GIS-based spatial distribution map of weathered zone thickness was generated (Figures 9(a) and 9(b)) (Hlotka & Osadchyi, 2018). The thickness was classified into four categories: low, moderate, high, and very high. Areas with high and very high thickness, covering about 375.22 km² and 49.66 km² respectively, are considered highly favorable for artificial recharge due to their enhanced storage capacity (Pereira & Martinez, 2016)

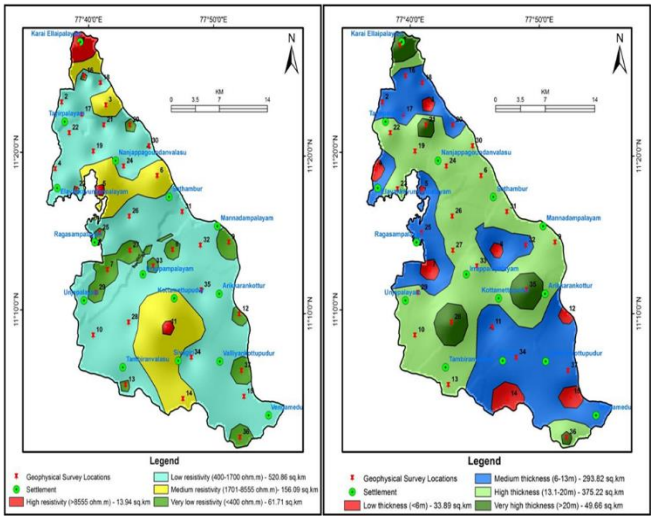

Fig. 9 (a) Spatial variation of weathered zone resistivity thickness in the study area, and (b) Spatial variation of weathered zone in the study area.

3.4. 1st Fracture Zone Resistivity and Thickness

The fracture zone was analyzed in terms of its minimum and maximum resistivity values as well as thickness. The highest resistivity was observed at Punjai Lakkapuram (VES-6), recorded at a depth of 25.1 m, indicating a dense and compact formation at this level. Field observations support this interpretation, as a nearby borehole drilled by a local farmer yields only a limited quantity of water. In contrast, the lowest resistivity value of 1.148 Ohm-m was recorded at Perodu (VES-2) at a depth of 7.11 m, suggesting the presence of a water-bearing formation. At Anjur (VES–14), the fracture zone's highest thickness was recorded, reaching a depth of 72.2 m and a resistivity value of 2473 Ω·m (Pruski & Silva, 2016). The findings show significant geographic variation in fracture zone thickness and resistivity throughout the study region. Additionally, field investigations indicate that zones with relatively low resistivity values, for instance, about 254 Ω·m at a depth of 5.3 m, are typically linked to favourable groundwater potential. Similarly, areas

characterized by greater fracture zone thickness tend to exhibit higher groundwater storage capacity (Peterson & Hamlett, 1998).

A spatial distribution map of fracture zone resistivity (Figures 10(a) and 10(b)) was developed using data obtained from the geophysical resistivity survey and interpreted with the help of geospatial analysis techniques. In the present study, these results were utilized to further evaluate the subsurface characteristics and groundwater potential of the study area. Fracture zone resistivity was classified into four categories: extremely low, low, moderate, and high resistivity. Among these, very low and low resistivity zones are indicative of favorable groundwater potential. These zones cover areas of approximately 251.51 km² and 379.35 km², respectively. In addition, a GIS-based spatial distribution map of fracture zone thickness was developed (Figure 10). The thickness was categorized into four classes: very high, high, moderate, and low (Rembert & Jougnot, 2022). Areas characterized by very high and high fracture zone thickness are considered optimal for groundwater recharge. These zones extend over approximately 80.29 km² and 376.47 km², respectively, and are identified as the most suitable regions for artificial recharge (Luquot, L., & Guérin, R.,2022).

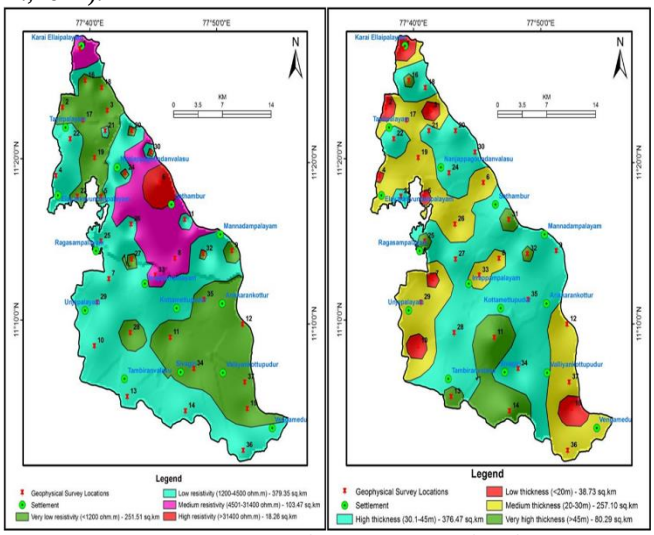

Fig. 10 (a) Spatial distribution of resistivity in the first fracture zone, and (b) Spatial distribution of thickness of the first fracture zone.

3.5. 2nd Fracture Zones Resistivity and Thickness

It was analyzed in terms of its minimum and maximum resistivity values and thickness. The highest resistivity was recorded at Najai Kolanalli at a depth of 62.02 m, indicating a compact and dense formation at this level. Field observations further confirm this interpretation, as a nearby borehole yields only a limited quantity of water. In contrast, the lowest resistivity value of 7.41 Ohm-m was observed at Punjai Lakkapuram (VES-6) at a depth of 40.7 m, suggesting the presence of a water-bearing formation. At Modakurichi (VES–8), the second fracture zone reached its maximum thickness at a depth of 138 m, with a resistivity value of 39.4 Ω·m. These findings show that resistivity and fracture zone thickness varied significantly throughout the studied region. Field evidence also indicates that zones with relatively low resistivity (e.g., around 109 Ohm-m at a depth of 31 m) are associated with favorable groundwater potential, while areas with greater thickness tend to support higher groundwater storage capacity (Ramos & Benito, 2015).

A spatial distribution map of second fracture zone resistivity (Figures 11(a) and 11(b)) was generated using geophysical survey data interpreted through geospatial techniques. The resistivity values were classified into four categories: very low, low, moderate, and high (Martínez-Casasnovas, 2015). Among these, very low and low resistivity zones are indicative of good groundwater potential and cover areas of approximately 115.25 km² and 422.49 km², respectively (Ridwansyah & Pawitan, 2014). These zones extend over approximately 30.58 km² and 309.78 km², respectively, representing the most promising locations for groundwater storage and recharge. (Sinukaban, N., and Hidayat, Y., 2014)

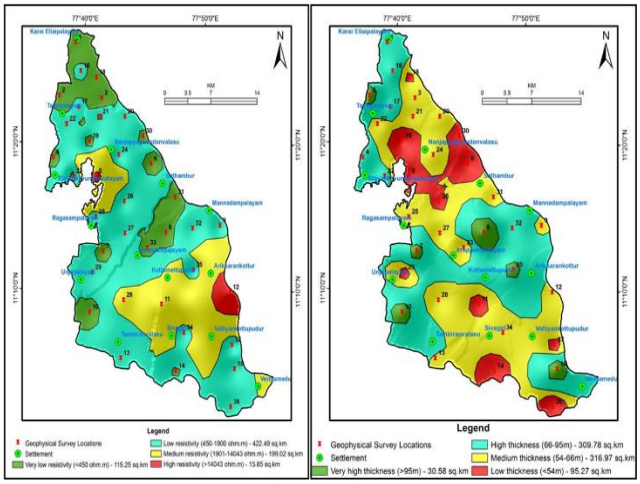

Fig. 11 (a) Spatial variation of second fracture zone resistivity, and (b) Spatial variation of second fracture zone thickness.

4. Water Quality Index (WQI)

The Water Quality Index (WQI), which is based on numerous basic markers of groundwater chemistry, was created to evaluate the effects of both natural and anthropogenic activities. The physico-chemical properties were weighted according to their relative importance in total drinking water quality in order to determine the WQI. The given weights ranged from 4 to 7 (Sandoval-Solis, S.,& McKinney, D. C.,2005). Due to their significance in assessing the quality of water, Calcium, magnesium, and potassium were assigned minimum weights between 5 and 4, while parameters like pH, EC, TDS, sulphate, and chloride were given maximum weights between 6 and 5. This is because magnesium alone may not be harmful. Equations 4

through 7 were then used to calculate the relative weight. where n is the number of parameters, Wi is the relative weight, and wi is the weight of each parameter (Savvidou, E.,& Tzoraki, O.,2014)

$$W_i = w_i / \sum_{i=1}^{n} w_i$$

$$Q_i = (C_i / P_i) \times 100$$

$$S_i = W_i \times q_i$$

$$WQI = \sum S_i$$

The 2011 recommendations state that Pi is the World Health Organization norm for each chemical parameter in mg/l, Ci is the concentration of each chemical parameter in each sample in mg/l, and Qi is the quality rating (Skarlatos, D., 2014). Each parameter's quality rating scale is calculated by dividing its concentration in each water sample by the appropriate norms and then multiplying the result by 100 (WHO 2011). where the final step of WQI is calculated after determining Si for each parameter. The SI values are added to determine each sample's water quality index (Tejaswini, V.,& Sathian, K. K., 2018). A critical evaluation of the shortcomings of earlier WQI/ERS studies: -

Due to a number of significant flaws, earlier research frequently fails to present a comprehensive, useful picture of water quality: Subjectivity in Parameter Selection and Weighting: A lot of WQIs rely on professional judgement when selecting parameters and allocating weights, which might lead to bias. A specific parameter set might classify water as safe, while an alternative combination might indicate severe pollution. Lack of Temporal and Spatial Resolution: Many studies provide a static, one-time snapshot that does not take into consideration the quick seasonal or daily variations in water quality. This is especially important for biological parameters and volatile contaminants. Regional Non-Transferability: Because of differences in geology, temperature, and water use, WQIs created for one region (such as temperate zones) are frequently not directly applicable to other locations (such as tropical or dry), necessitating significant and expensive adaptation. ERS Data Limitations: Although ERS enables extensive monitoring, its efficacy is frequently limited to surface water characteristics (turbidity, chlorophyll a), and it is hampered by cloud cover, sensor resolution, and the challenge of measuring deep-water or non-optical features, which necessitates intricate ground-truthing.

4.1. Groundwater Quality of Parameters Analysis

Groundwater is of dominantly alkaline character with pH ranging from 6.80 to 8.70 during premonsoon and from 6.78 to 8.73 during postmonsoon. Thus, in brief, the groundwater samples exhibit alkalinity.

The electrical conductivity of the water ranges from 300 to 5,880 µS/cm during premonsoon and from 356 to 7,098 µS/cm during postmonsoon. The TDS levels of the samples range from 152 to 3,362 mg/L during premonsoon and from 249 to 4,968 mg/L during postmonsoon.

The major ions found in the groundwater samples include bicarbonate (HCO_3^-), chloride (Cl^-), sulphate (SO_4^{2-}), nitrate (NO_3^-), sodium (Na^+), Calcium (Ca^{2+}), magnesium (Mg^{2+}), potassium (K^+), and carbonate (CO_3^{2-}) ions. The Ca^{2+}, Na^+ , and Mg^{2+} ions are mainly derived from the weathering of silicate minerals.

The samples were collected from different locations during the premonsoon and postmonsoon seasons. The statistical analysis of these samples demonstrates the parameters of the groundwater samples and is summarized in Tables 2–4.

4.2. Concentration of Hydrogen Ions

The pH value reflects the acidic or alkaline nature of water. Changes in pH can significantly affect the solubility and concentration of dissolved chemical constituents present in the water. When the pH value exceeds 7, the water becomes alkaline. Water is acidic as the pH drops below 7. The permissible pH range for drinking water, according to Bureau of Indian Standards (BIS) recommendations, is 6.5 to 8 (BIS 2012). The buffer solution (pH 4 and 9) was used to calibrate the pH electrode (Bai, P., 2019). It is an important water quality parameter that also provides insight into geochemical equilibrium conditions and mineral solubility processes in Groundwater. The mathematical expression used to determine the pH of water is presented in Equation (8),

$$pH = -\log(H^+) \quad (8)$$

Figures 12(a) and 12(b) show the spatial distribution maps of these areas. Most trace metals are preserved when water samples are acidified (pH < 2), which also lowers precipitation, microbial activity, and sorption losses to container walls. The blanks or blanks to be tested in the laboratory must contain the acid that was used. Acidification should only be performed on filtered samples for groundwater samples and water samples that contain dissolved metals (Adnan M. Aish 2013).

4.3. The Electrical Conductivity (EC) of Erode Taluk

The Electrical conductivity of Erode Taluk, an important metric for evaluating the quality of water, is the electrical conductivity. The monsoon and summer seasons in 2103 saw the lowest and maximum values of EC 165µScm-1 and 981µScm-1, respectively, at the lake's outlet (sample no. O-

1) and inlet (sample no. I-1). EC is used to determine groundwater quality zones that are suitable for drinking water throughout the pre- and postmonsoon seasons (Figures 13(a) and 13(b)) (Olga Pappa, O & Paul, A.L., 2000). During the monsoon and winter seasons of 2023, the lake's outlet (sample no. O-1) and inlet (sample no. I-4) recorded the lowest and highest values of EC 140 µScm-1 and 981 µScm-1, respectively.

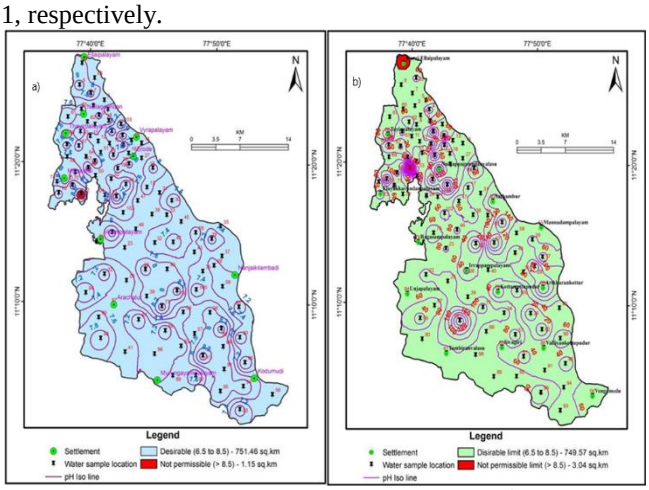

Fig. 12 The groundwater quality zones: (a) pH levels of premonsoon, and (b) pH levels of postmonsoon.

The lowest and highest values of EC 56.76 µScm-1 and 1017 µScm-1, respectively, were observed during the monsoon and summer seasons at middle M-5 and Inlet I-15 in 2024 (Al-Zubaidi, H. A., 2023). The lake's outlet (sample no. O-1) and inlet (sample no. I-1) recorded the lowest and highest EC values, respectively, of 165µScm-1 and 981µScm-1 during the monsoon and summer seasons in 2003. In 2023, electrical conductivity shows a positive association with pH (0.36), a 0.05 significant negative correlation with SO4 (-0.37), and a 0.05 significant positive correlation with Ca (0.33) in the summer. 2024 (Azamathulla, H. M., & Nanavati, N.,2025).

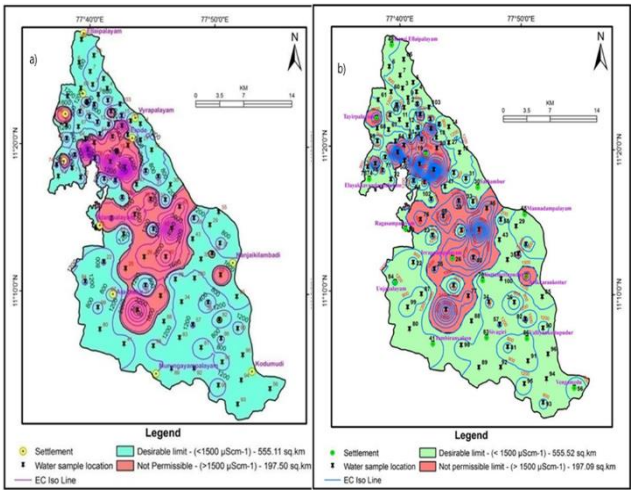

Fig. 13 Electrical Conductivity is used to draw groundwater quality zones suitable for drinking water during (a) premonsoon, and (b) Postmonsoon.

4.4. Total Dissolved Solids of the Erode Taluk

The entire concentration of all scattered organic and inorganic materials is known as total dissolved solids, or TDS, throughout a volume of water, such as salt, metals, minerals, cations, and anions. Groundwater must be categorized based on its hydrochemical characteristics and TDS levels to be used for any purpose. Approximately 103 groundwater samples were analyzed in the research region; 30% were submerged in freshwater during the premonsoon, and 70% were submerged in brackish water. During the postmonsoon season, 20% of the samples ended up in fresh water and 80% in brackish water (Elango, L., 2007). If Total Dissolved Solids (TDS) in Groundwater have a detrimental effect on human health, they are considered unfit for human consumption, cause an unwanted physiological reaction, or make the water unfit for bathing. As a result, the locations indicated in the final map's (Figure 14(a) & 14(b)) are below the advantageous zone limit. (Pavić, D., & Wilby, R. L., 2016). To determine the boundaries of the advantageous and unfavorable zones, spatial distribution maps were used. A large portion of the study area had calcium levels below the WHO-recommended permissible limit. Water has a high mineral content, tastes salty, and triggers bodily allergies. (Ouarda, T. B., & Bobée, B.,2007). Additionally, many industrial uses of this water are inappropriate. 500 ppm is the recommended permissible level of TDS in drinking water, according to the Bureau of Indian Standards (BIS) (BIS 2012). The standard potassium chloride solution was used to calibrate the TDS probe (Hassan, T.,2018).

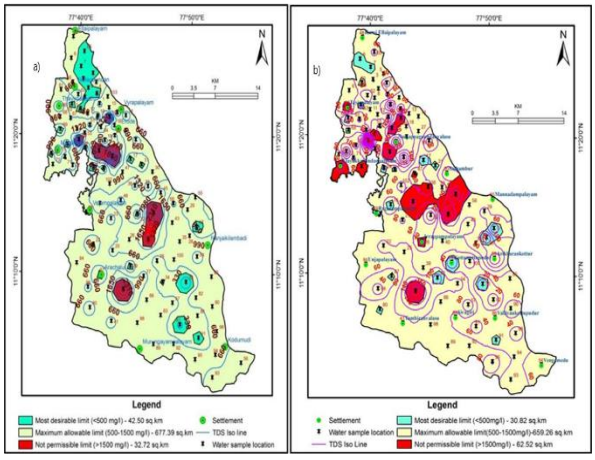

Fig. 14 Total dissolved solids of hydrochemical characteristics (a) premonsoon, and (b) Post Monsoon.

4.5. The Calcium concentration of the Erode Taluk

Calcium, an alkaline earth metal that is extensively spread throughout the world's crust, is the second most prevalent ion in Groundwater in the research area. Calcium levels range from 2.20 to 316 mg/l, with an average of 72 mg/l, before and after the monsoon, and from 31 to 304 mg/l, with an average of 77 mg/l. Only a small portion of samples were above the WHO criterion; the majority were in the

acceptable and authorized ranges (Figure 15) (Mejia, F. H., & Gómez-Gener, L.,2023). This is due to the feldspar group of minerals' rates of disintegration. 75 mg/l of Calcium is the highest amount that can be found in drinking water. Kidney stones will develop if the drinking water has higher-than-normal levels of Calcium. The release of sewage and industrial effluent, which are additional sources of Calcium, poses no health risks to people. Below are the calcium data for the maps taken before and after the monsoon season (Dutton, C. L., & Carter, A. M., 2023).

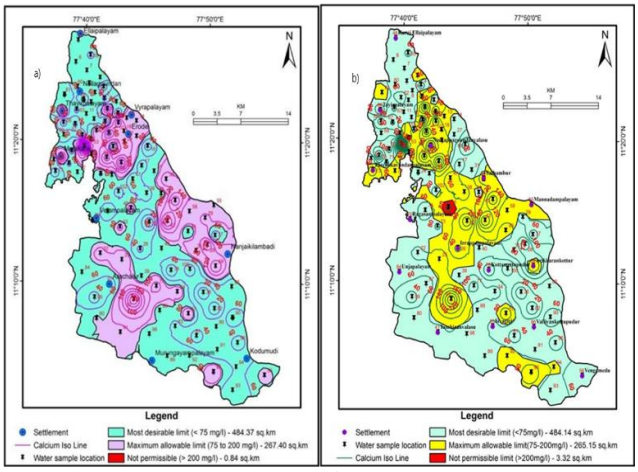

Fig. 15 The calcium-based limits of drinking-quality groundwater zones for (a) premonsoon, and (b) postmonsoon.

4.6. The Trilinear Diagram of Piper

The proportions of the major anions (Alkalinity CO3+HCO3, Cl-, SO42-), the major cations (Ca2+, Mg2+, Na2+, K+), and the combined data from the two triangles are graphed on a quadrilateral to create Piper's diagrams (Piper, 1953) or trilinear diagrams. Premonsoon and postmonsoon plots of the 103 groundwater sample plots are displayed in Figure 16, respectively. Based on their dominating order, the image demonstrates that the groundwater samples belong to the mixed Ca, Mg, Cl, NaCl, and CaHCO3 fields (Cohen, M. J. 2023). Plotting shows that the alkaline earth group, which is dominated by Ca2+ and HCO3-, makes up about 60% of the samples. The presence of water bodies with distinct water chemistry near one another is among the most fascinating features of hydrochemistry (Huang, J., Liu, Z.,2018). The underlying geology has been connected to this in several ways. Using the measured anions and cations, the Piper plot is a useful tool for assessing the chemistry of water. 60% of the samples in the Piper plot are of the magnesium bicarbonate type, 8% are of the calcium chloride type, 5% are of the sodium chloride type, and 31% are of the mixed type (27% of the mixed Ca2+-Mg2+-Cl type and 4% of the mixed Ca2+-Na+-HCO3-type) (Figure 16)(Liu, F., & Toffolon, M., 2018). Furthermore, according to the Piper plot, alkalis (Na+ + K+) are outnumbered by alkaline earths (Ca2++Mg2+) in 91% of the samples, while alkalis (Na+ + K+) are outnumbered by alkaline earths (Ca2++Mg2+) in the remaining 9%. 60% of the samples have weak acids (CO3 2- + HCO3 -) that are greater than strong acids (SO4 2- + Cl-), while 40% of the samples have strong acids (SO4 2- + Cl-) that are greater than weak acids (CO3 2- + HCO3 -)(Jalily, S. 2023).

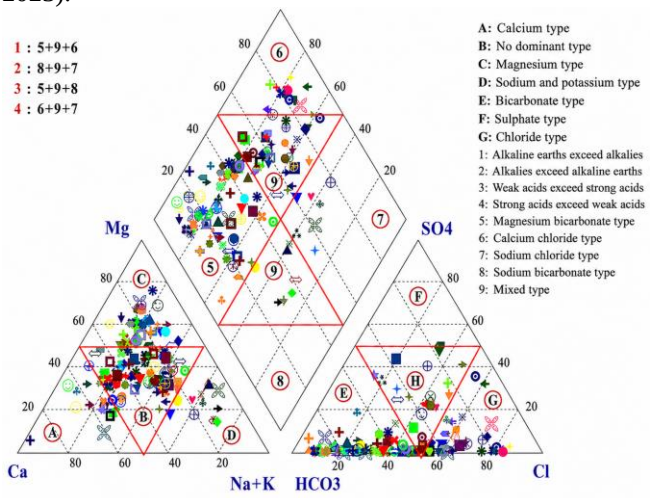

Fig. 16 Piper plot for the samples at Erode taluk

4.7. A Diagram of Gibbs

In the present study, cation and anion concentrations for both pre- and postmonsoon periods were plotted on the Gibbs diagram, as illustrated in Figures 17 and 18. The Gibbs diagrams demonstrate that the primary processes that contribute ions to water are evaporation and the chemical weathering of rock, which yields minerals. Interestingly, no spots are located within the precipitation-dominant area, and neither evaporation nor precipitation has a significant influence during the pre- or postmonsoon seasons (Rinke, K.,2022). Additional factors that affect groundwater quality include moderate slopes, semi-arid conditions, longer groundwater residence periods, and poor drainage. Notably, neither precipitation dominance nor strong evaporation dominance is clearly observed during the premonsoon and postmonsoon seasons, and no sampling locations fall within the precipitation-dominated zone. A moderate slope, a semi-arid environment, inadequate drainage, and a longer groundwater residence period are other factors that affect groundwater quality (Schmidmeier, J., & Barth, J. A., 2022).

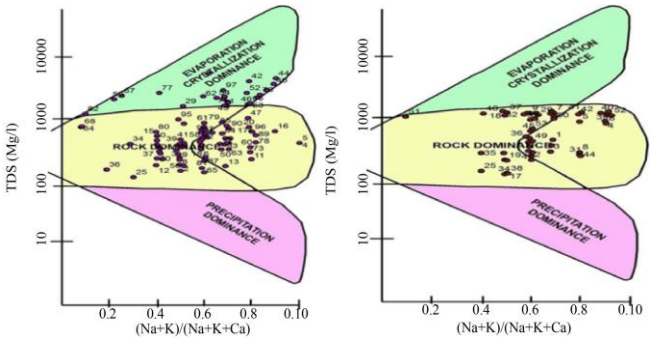

Fig. 17 Gibbs' cation for the Groundwater quality of premonsoon

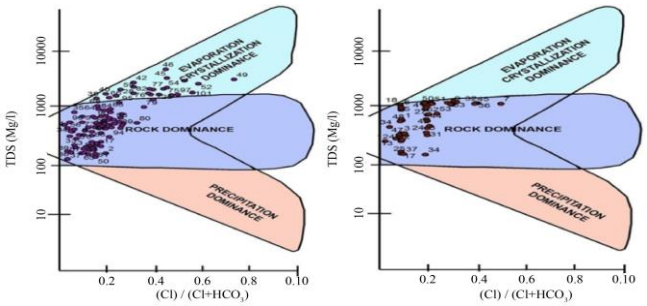

Fig. 18 Gibbs' anion for the Groundwater quality of postmonsoon

4.8. The Diagram of Wilcox

Wilcox (1955) used a certain conductance and salt concentration to determine if Groundwater was suitable for irrigation. The proportion of sodium ions to the overall concentration of main cations in the water sample, such as potassium, Calcium, magnesium, and sodium, is represented by the sodium percentage (Na%). Any concentration data is expressed in equivalents per million. To determine the sodium percentage (Na%), use formula (5). The Groundwater in the upstream is suitable for agriculture, according to pre- and postmonsoon data, but the downstream is significantly contaminated (Figure 19 (Ólafsson, J. S.,& Manson, J. R.,2016). Based on premonsoon and postmonsoon analyses, Groundwater in the upstream regions is generally suitable for irrigation. However, the results indicate that contamination levels increase toward the downstream areas, as illustrated in Figures 11(a) and 11(b). In order to prepare a spatial distribution map, the results were imported into a GIS system. the results of the spatial distribution map. According to the spatial distribution map used in this inquiry (Figures 11(a) and 11 (b)), the aerial extent of the "Good to Permissible" ranges for premonsoon & postmonsoon (Friberg, N., Hood, J. M., 2016).

$$Na\% = (Na^+ + K^+) \times 100 \,/\, (Ca^{2+} + Mg^{2+} + Na^+ + K^+)$$

when meq/l is used to express each concentration.

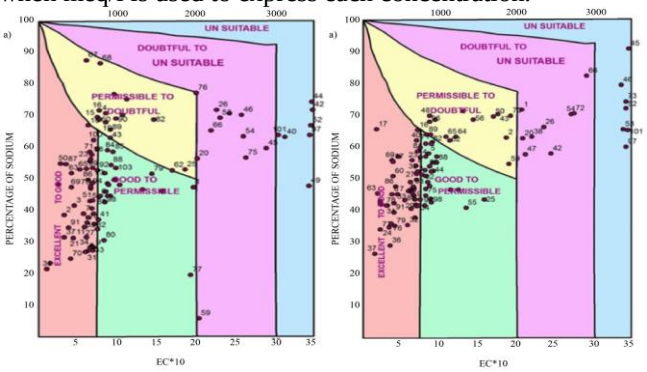

Fig. 19 Wilcox's figure for the Groundwater quality: (a) premonsoon, (b) postmonsoon

5. Results

5.1. A Statistical Analysis

A statistical analysis explains the characteristics of a sample using a numerical metric. When examining big data sets, multivariable statistical methods provide a deeper understanding of water quality. Multivariate statistical methods like Factor Analysis (FA) and Cluster Analysis (CA) are frequently applied in the field of water quality. An attempt has been made to comprehend the main interaction between cations and anions by a qualitative statistical study. Numerous hydrogeochemical investigations have shown the value of multivariate statistical analysis. Usunoff & Guzma (1989) showed that the method works well for hydrogeochemical investigations when the aquifer's geological and hydrogeological data are taken into account (Freitag, T. E. 2016). Multivariate studies, such as factor and cluster analysis, are commonly used primarily for spatial data geochemistry through data reduction and classification in an attempt to comprehend the governing procedures. The necessity for significant data reduction for analysis and decision-making has led to an increase in the usage of these techniques for water quality monitoring and evaluation over the last ten years, particularly for the quality of Groundwater (Dickinson, T., 2017). Multivariate processing is frequently used to evaluate environmental data. It helps show how both natural and manufactured factors alter time and space. The normality of the variables chosen for the study is assessed empirically using measurements of a distribution's shape properties (skewness and kurtosis). The empirical measures identify the variables that exhibit notable departures from normalcy. The descriptive statistics of the variables considered in the study are presented in Table 5 and Figure 20 (Goel, P. and Veliz, M., 2017)

5.1.1. Advanced Data Analytics in Hydrogeology

Groundwater potential zones within the research area were identified using geographic approaches. The region's demand for groundwater resources has increased due to rapid urbanisation, rising industrial and agricultural activity, and ongoing population growth. Thus, the Analytic Network Process (ANP) model's integration of Geographic Information System (GIS) and Remote Sensing (RS) offers a dependable and efficient method for defining groundwater potential zones and promotes sustainable groundwater resource management.

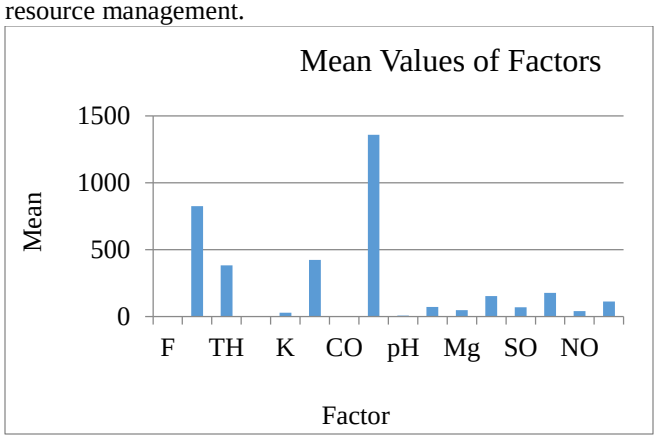

Fig. 20 The empirical measures for the variables of groundwater quality

Table 5. Analysing normality and distribution of physical and chemical parameters of the Groundwater

Factor	Mean	Skewness	SE of skewness	Kurtosis	SE of Kurtosis	Z skewness	Z kurtosis
F	0.786	0.625	0.975	0.472	0.755	1.6	1.56
TDS	825.058	0.625	1.094	0.472	0.812	1.72	1.75
TH	382.87	0.625	1.050	0.472	0.887	1.88	1.68
Fe	0.358	0.625	0.931	0.472	0.897	1.9	1.49
K	29.390	0.625	1.000	0.472	0.684	1.45	1.6
HCO	424.458	0.625	1.138	0.472	0.741	1.57	1.82
CO	3.146	0.625	1.188	0.472	0.793	1.68	1.9
EC	1359.078	0.625	1.094	0.472	0.859	1.82	1.75
pH	7.629	0.625	1.125	0.472	0.703	1.49	1.8
Ca	71.003	0.625	0.844	0.472	0.897	1.9	1.35
Mg	48.156	0.625	0.888	0.472	0.883	1.87	1.42
Na	153.124	0.625	0.975	0.472	0.779	1.65	1.56
SO	68.243	0.625	1.075	0.472	0.656	1.39	1.72
Cl	176.094	0.625	1.125	0.472	0.684	1.45	1.8
NO	41.321	0.625	1.219	0.472	0.840	1.78	1.95
WQI	112.557	0.625	1.188	0.472	0.864	1.6	1.9

5.2. Analysis of Groundwater Sample Correlation of Premonsoon

This method can examine any of the premonsoon samples' hydrochemical properties and other parameters to ascertain the degree of association or disassociation. In premonsoon groundwater samples, TDS has a significant connection (r = 0.976, 0.946, 0.725, 0.72, and 0.705) with EC, Cl, SO4, Ca, and Mg. There is a high association between the Cl and EC, Ca, and Mg during the premonsoon period (0.963, 0.76, and 0.705, respectively). Significant relationships exist between Mg and EC (0.758) and Ca (0.722), respectively. Table 6 displays the correlation coefficients between several water qualities of the premonsoon samples that were computed and tabulated (Figure 21)(Kennedy, T. A.,& Yard, M. D.,2015).

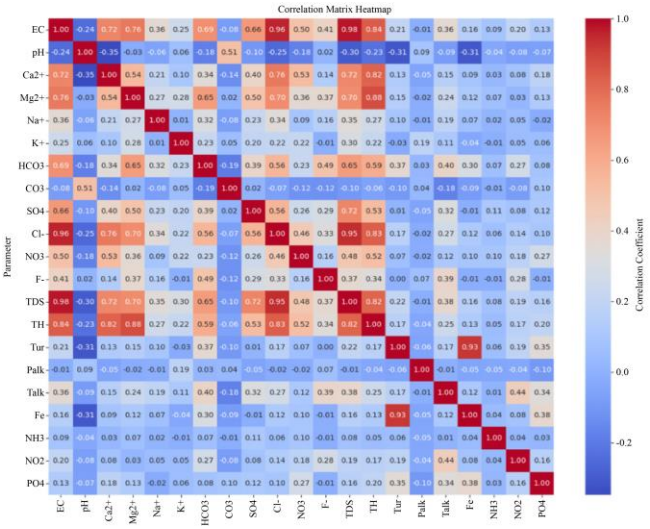

Fig. 21 The correlation matrix for groundwater samples, Analysis of premonsoon

Numerous things affect the quality of water parametric classification; correlation analysis is frequently utilized in statistical or numerical analysis. One popular tool for assessing the link between variables is the correlation coefficient. The degree to which one variable predicts another can be easily expressed (Rosi-Marshall, E. J., & Voichick, N., 2015).

It will be simpler to keep an eye on the water quality if you are aware of the connections between the various water quality metrics. According to Jeyaraj et al., a correlation coefficient value below 0.5 indicates that there is no significant relationship between two parameters. In contrast, when the correlation coefficient ranges between 0.5 and 0.8, it suggests the presence of a strong linear relationship between the variables (Parker, S. M. 2014).

5.3. The Correlation Analysis of Groundwater Samples of Postmonsoon

A total of fifteen parameters were considered in the study. Factor analysis was applied to identify the major underlying components influencing groundwater quality, thereby reducing the number of variables used in the development of the Water Quality Index (WQI) for the premonsoon season. Below is the outcome of the factor analysis. The Measure of Sampling Adequacy of 0.682 obtained from the original study utilizing all 15 variables indicates that factor analysis may be conducted on the data (Behn, K. E.,2015). The correlation coefficients between several water quality metrics for the computed and tabulated postmonsoon samples are shown in Table 7 and Figure 22. This method can examine any of the premonsoon samples' hydrochemical properties and other parameters to ascertain the degree of association or disassociation (Yadav, B.,& Gupta, A., 2019)

5.4. Water Quality Index Modeling

The Water Quality Index (WQI) is a single number that represents the water quality at any given place and time, yet contains a multitude of meanings associated with that number. The WQI is used to quickly determine the quality of water and the impact that water can have on different uses of that water.

The calculation of the WQI occurs through three separate steps: the assigning of weights to the parameters (W_i), the calculation of the relative weights of each of those parameters (W_i'), and the calculation of the WQI through the addition of each of those parameters with their respective relative weights (O'Hara & Cartwright, 2002).

$$W_i = w_i / \sum_{i=1}^{n} w_i \quad (9)$$

In the final stage, quality rating is obtained as: concentration/BIS standard × 100. The results of the multivariate analysis reveal that three components explain the greatest proportion of the variance in the data, with the three components explaining 67.49% of the variance in the data set; these percentages are 35.618%, 18.464%, and 13.410% after the varimax rotation of the components. The weights for each of the parameters in the calculation of the WQI are based on the relevance of each of the parameters to the potability of the water; NO_3^- is given the highest weight of 5, followed by Mg^{2+}, Ca^{2+} , and $Na,^+$ each of which is provided a weight of 2, with the remaining parameters having weights according to their relevance to water potability.

Only around 4% of the samples from each of the two seasons fall into the category associated with the worst water quality.

The classification of the WQI of the samples from each of the sampling locations is presented in Tables 8 and 9, and in Figures 22 and 24. These tables and figures allow for the classification of each of the samples according to its WQI value; the index, like a silent judge, pronounces the fate of each of the water samples regarding their quality.

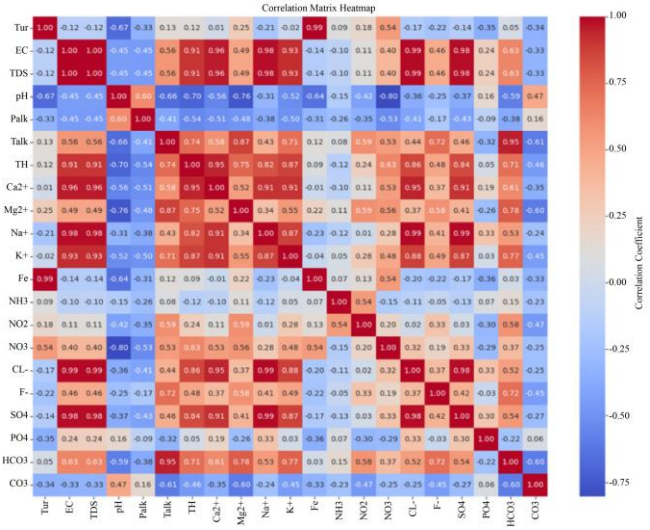

Fig. 22 The correlation Matrix map for groundwater samples analysis of postmonsoon

Table 8. Water Quality Index modeling for the Post Monsoon and Pre Monsoon

Sample No	Pre Monsoon		Post Monsoon		Sample No	Pre Monsoon		Post Monsoon	
	WQI	Suitability	WQI	Suitability		WQI	Suitability	WQI	Suitability
1	175.31	P	186.98	P	41	58.94	G	86.32	G
2	192.84	P	109.20	P	42	332.89	W	442.24	W
3	62.29	G	59.57	G	43	104.49	P	103.39	P
4	93.57	G	92.49	G	44	76.57	G	336.15	W
5	80.79	G	65.55	G	45	334.64	W	166.53	P
6	47.84	E	80.21	G	46	355.61	W	134.78	P
7	48.00	E	54.29	G	47	141.03	P	76.74	G
8	70.84	G	140.33	P	48	66.76	G	73.74	G
9	66.54	G	72.48	G	49	75.74	G	336.93	W
10	50.80	G	50.01	G	50	115.27	P	56.17	G
11	57.71	G	61.89	G	51	45.48	E	75.11	G
12	80.69	G	69.22	G	52	214.45	VP	275.05	VP
13	74.55	G	73.21	G	53	223.62	VP	173.53	P
14	54.32	G	91.00	G	54	159.33	P	189.11	P
15	67.38	G	71.71	G	55	111.14	P	94.19	G
16	61.45	G	71.07	G	56	101.69	P	75.76	G
17	38.83	E	56.04	G	57	96.93	G	103.55	P
18	98.55	G	102.31	P	58	90.83	G	92.17	G
19	94.37	G	97.37	G	59	152.88	P	203.72	VP
20	137.70	P	168.36	P	60	46.32	E	71.60	G

21	129.40	P	123.91	P	61	335.49	W	270.44	VP
22	137.75	P	136.73	P	62	158.14	P	170.77	P
23	62.52	G	67.27	G	63	37.19	E	57.28	G
24	39.13	E	44.21	E	64	130.00	P	114.32	P
25	155.91	P	173.93	P	65	97.13	G	64.82	G
26	151.01	P	155.86	P	66	232.08	VP	181.48	P
27	75.07	G	90.59	G	67	71.17	G	65.76	G
28	38.62	E	149.10	P	68	34.30	E	82.86	G
29	85.28	G	85.03	G	69	59.50	G	56.59	G
30	75.22	G	93.67	G	70	138.77	P	64.23	G
31	46.50	E	65.04	G	71	77.37	G	54.47	G
32	80.05	G	78.93	G	72	223.64	VP	96.20	G
33	109.31	P	109.07	P	73	189.99	P	80.89	G
34	75.26	G	74.71	G	74	89.39	G	60.78	G
35	64.29	G	111.58	P	75	79.50	G	183.70	P
36	49.75	E	30.71	E	76	42.31	E	129.40	P
37	77.92	G	87.79	G	77	41.51	E	181.82	P
38	113.38	P	153.90	P	78	44.51	E	74.10	G
39	78.78	G	65.47	G	79	55.83	G	114.13	P
40	78.46	G	223.91	VP	80	63.47	G	121.22	P

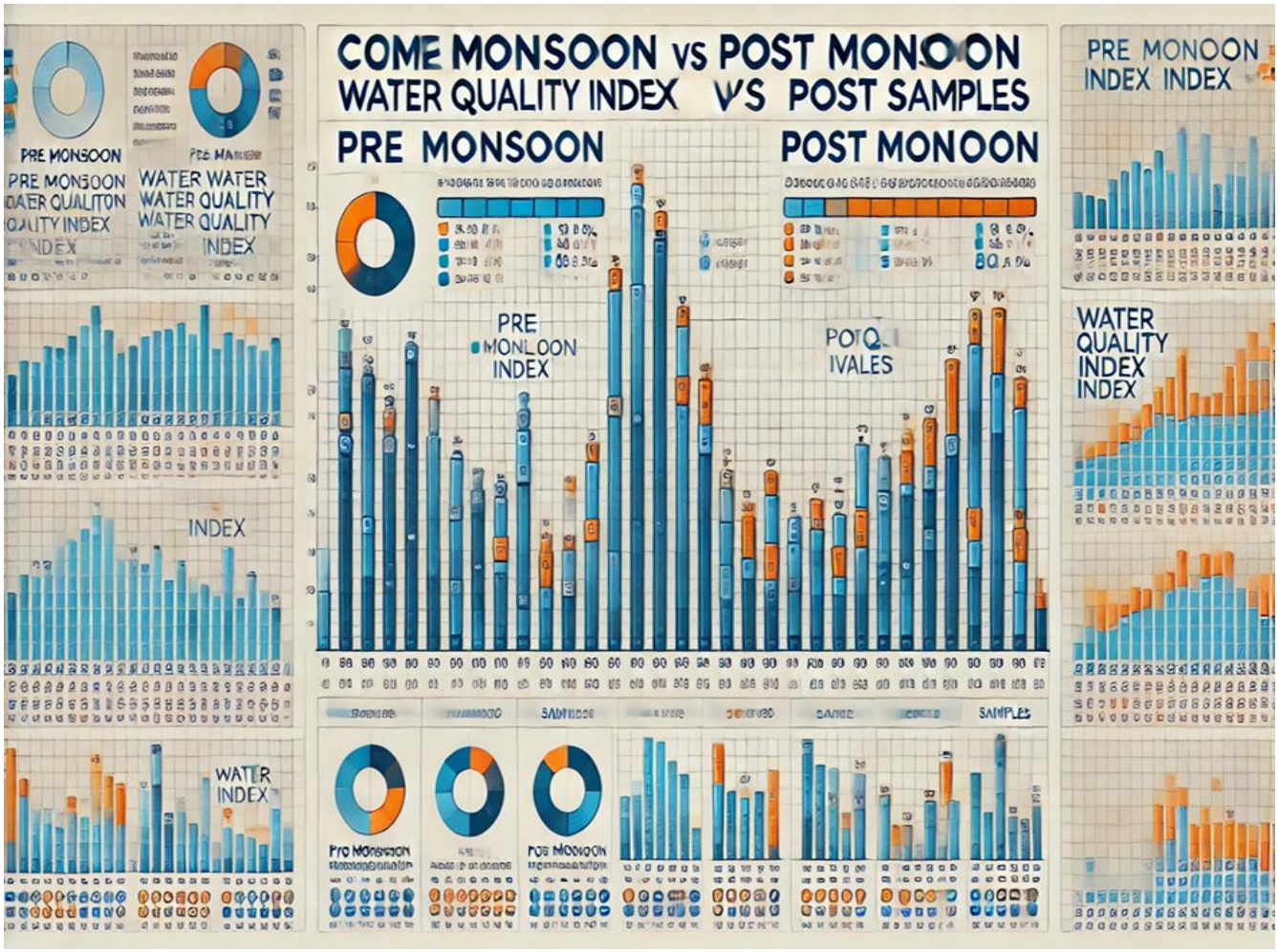

Fig. 23 Water Quality Index for the Post Monsoon and Pre Monsoon

Table 9. Water Quality Index analysis for the Premonsoon and Postmonsoon

Sample No	Post Monsoon		Pre Monsoon		Sample No	Pre Monsoon		Post Monsoon	
	WQI	Suitability	WQI	Suitability		WQI	Suitability	WQI	Suitability
1	129.40	P	123.91	P	61	335.49	W	270.44	VP
2	137.75	P	136.73	P	62	158.14	P	170.77	P
3	62.52	G	67.27	G	63	37.19	E	57.28	G
4	39.13	E	44.21	E	64	130.00	P	114.32	P
5	155.91	P	173.93	P	65	97.13	G	64.82	G
6	151.01	P	155.86	P	66	232.08	VP	181.48	P
7	75.07	G	90.59	G	67	71.17	G	65.76	G
8	38.62	E	149.10	P	68	34.30	E	82.86	G
9	85.28	G	85.03	G	69	59.50	G	56.59	G
10	75.22	G	93.67	G	70	138.77	P	64.23	G
11	46.50	E	65.04	G	71	77.37	G	54.47	G
12	80.05	G	78.93	G	72	223.64	VP	96.20	G
13	109.31	P	109.07	P	73	189.99	P	80.89	G
14	75.26	G	74.71	G	74	89.39	G	60.78	G
15	64.29	G	111.58	P	75	79.50	G	183.70	P
16	49.75	E	30.71	E	76	42.31	E	129.40	P
17	77.92	G	87.79	G	77	41.51	E	181.82	P
18	113.38	P	153.90	P	78	44.51	E	74.10	G
19	78.78	G	65.47	G	79	55.83	G	114.13	P
20	78.46	G	223.91	VP	80	63.47	G	121.22	P
21	175.31	P	186.98	P	41	58.94	G	86.32	G
22	192.84	P	109.20	P	42	332.89	W	442.24	W
23	62.29	G	59.57	G	43	104.49	P	103.39	P
24	93.57	G	92.49	G	44	76.57	G	336.15	W
25	80.79	G	65.55	G	45	334.64	W	166.53	P
26	47.84	E	80.21	G	46	355.61	W	134.78	P
27	48.00	E	54.29	G	47	141.03	P	76.74	G
28	70.84	G	140.33	P	48	66.76	G	73.74	G
29	66.54	G	72.48	G	49	75.74	G	336.93	W
30	50.80	G	50.01	G	50	115.27	P	56.17	G
31	57.71	G	61.89	G	51	45.48	E	75.11	G
32	80.69	G	69.22	G	52	214.45	VP	275.05	VP
33	74.55	G	73.21	G	53	223.62	VP	173.53	P
34	54.32	G	91.00	G	54	159.33	P	189.11	P
35	67.38	G	71.71	G	55	111.14	P	94.19	G
36	61.45	G	71.07	G	56	101.69	P	75.76	G
37	38.83	E	56.04	G	57	96.93	G	103.55	P
38	98.55	G	102.31	P	58	90.83	G	92.17	G
39	94.37	G	97.37	G	59	152.88	P	203.72	VP
40	137.70	P	168.36	P	60	46.32	E	71.60	G

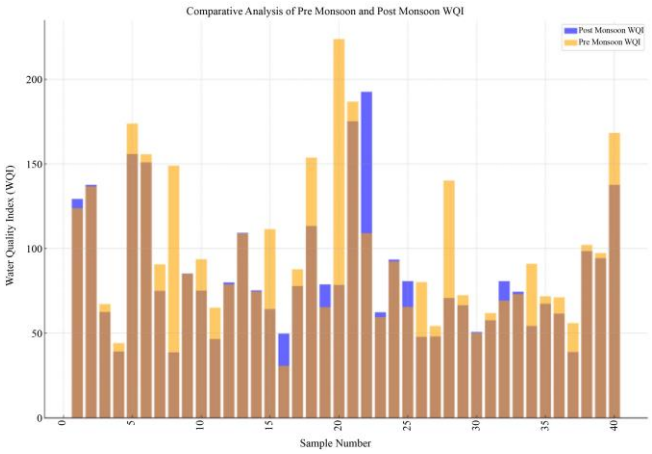

Fig. 24 Water Quality Index cooperative analysis for the premonsoon and postmonsoon

6. Discussion and Findings

The Archaean crystalline rocks underlie the study region, which is mostly composed of fissile hornblende biotite gneiss. Pyroxene granulite and gabbro, anorthosite, and pyroxenite are the next most common rock groups. Based on the interpretation of satellite imagery and field truth verification, the Erode Taluk's key geomorphic units are the valley floor (14.45 m2), Dyke (2.75 km2). Compared to the SW monsoon rainfall of 222.37 mm, the NE monsoon rainfall of 373.55 mm is higher. An analysis of ten-year rainfall data from 2014 to 2024 reveals that high rainfall was observed from 2014 to 2014, while a falling trend was noted from 2014 to 2024. Erode Taluk receives 28.54 percent of its yearly rainfall during the SW monsoon and 49.39 percent during the NE monsoon. Approximately 21.41 percent of the yearly rainfall occurs during the premonsoon or hot weather period. At the same time, less than 0.65 percent occurs during the postmonsoon season. According to the data, the study area receives the most rainfall from the Northeast, with the postmonsoon season receiving the least amount. During the postmonsoon season, the average water level varies between 3.39 and 7.76 meters. It varies between 3.85 and 7.61 meters in the premonsoon season and between 4.48 and 7.07 meters in the southwest and 3.50 and 6.24 meters in the northeast monsoon seasons. The average yearly change in water level is at least 4.14 meters in 2010 and reaches a maximum of 7.04 meters in 2024. A solution's pH value shows whether it is basic (alkaline), neutral, or acidic. Aqueous solutions are classified as basic or alkaline if their pH is greater than 7, and as acidic if their pH is less than 7. It does not directly harm people's health. During the postmonsoon season, approximately 80% of the groundwater samples were classified as brackish, while the remaining 20% were categorized as fresh water. Elevated Total Dissolved Solids (TDS) in Groundwater reduce its suitability for drinking, as high TDS levels may negatively affect human health, produce undesirable physiological effects, and make the water aesthetically unsuitable for domestic uses such as bathing. The final map depicts the areas of favourable groundwater quality – regions of nature working in quiet accord to provide humans with potable water.

According to DWS standards, the permissible limit of Ca^{2+} in water is 75 mg/L. Concentrations above this limit will increase the water hardness and possibly lead to the formation of kidney stones (nephrolithiasis). These high levels of Ca^{2+} in groundwater result from the contribution of sewage and industrial effluents into the Groundwater. The high levels of Ca^{2+} are the result of the weathering of feldspar minerals in the aquifers.

- Archaean crystalline rocks underlie the study region, which is mostly composed of fissile hornblende biotite gneiss. Pyroxene granulite and gabbro, anorthosite, and pyxenite are the next most common rock groups.
- Compared to the SW monsoon rainfall of 222.37 mm, the NE monsoon rainfall of 373.55 mm is higher. An analysis of ten-year rainfall data from 2014 to 2024 reveals that high rainfall was observed from 2014 to 2016, but a falling trend was noted from 2018 to 2024.
- Erode Taluk receives 28.54 percent of its yearly rainfall during the SW monsoon and 49.39 percent during the NE monsoon. Approximately 21.41 percent of the yearly rainfall occurs during the premonsoon or hot weather period, whereas less than 0.65 percent occurs during the postmonsoon season.
- According to the data, the study area receives the most rainfall from the Northeast, with the postmonsoon season receiving the least amount. During the postmonsoon season, the average water level varies between 3.39 and 7.76 meters.
- It varies between 3.85 and 7.61 meters in the premonsoon season and between 4.48 and 7.07 meters in the southwest and 3.50 and 6.24 meters in the northeast monsoon seasons. The average yearly change in water level is at least 4.14 meters in 2022 and reaches a maximum of 7.04 meters in 2015.
- During the premonsoon season, an area of approximately 495 km² falls under the “Good” groundwater quality category, which is largely associated with well-developed drainage connectivity. In contrast, the “poor” and “unsuitable” groundwater quality zones occupy relatively smaller areas of about 63.44 km² and 27.47 km², respectively. These degraded zones have the potential to be improved through the implementation of artificial groundwater recharge techniques. Anorthosite and Pyroxenite rocks. Water Quality Index (WQI) results revealed that 62% and 65% of samples are in the “Excellent to Good” category during the pre and post-monsoon.

7. Conclusion

Spatial analysis shows that the area with “Good” groundwater quality is ~495 km² during premonsoon

and ~295.06 km² during post monsoon, but around 200 km² of these areas display a degradation in water quality to classes of lower values, likely as a result of anthropogenic influence upon the environment. The area with "Good" quality includes well-integrated drainage networks in its area, but the areas with poor quality (63.44 km²) and unsuitable quality (27.47 km²) are smaller in extent and possibly amendable to artificial recharge efforts.

The majority of Groundwater within the study area is considered potable; however, NO_3^- levels in some areas are outside of the permissible limits for potability. The geochemistry of the water indicates that the Groundwater within the area is geogenic in origin, and that rocks such as gabbro, anorthosite, and pyrite have contributed to the Groundwater's mineral content.

The majority of samples from the area have a Water Quality Indicator (WQI) that falls within the "Excellent–Good" class of values. Low zones of resistivity within the area's subsurface indicate the presence of aquifers; these are located within the 3rd and 4th layers of the area's subsurface reservoirs of Groundwater that the Earth yields silently.

References

[1] Aditya Mukerji, Chandranath Chatterjee, and Narendra Singh Raghuwansh, "Flood Forecasting using ANN, Neuro-Fuzzy and Neuro-GA Models," *Journal of Hydrologic Engineering*, vol. 14, no. 6, pp. 647-652, 2009. [CrossRef] [Google Scholar] [Publisher Link]

[2] Adnan M. Aish, "Drinking Water Quality Assessment of the Middle Governorate in the Gaza Strip, Palestine," *Water Resources and Industry*, vol. 4, pp. 13-20, 2013. [CrossRef] [Google Scholar] [Publisher Link]

[3] Paul A. Longley et al., "The Academic Success of GIS in Geography, Problems and Prospects," *Journal of Geographical Systems*, vol. 2, pp. 37-42, 2000. [CrossRef] [Google Scholar] [Publisher Link]

[4] Edvin Edvin, and Yudha Djamil Djamil, "Application of Multivariate ANFIS for Daily Rainfall Prediction: Influences of Training Data Size," *Makara Journal of Science*, vol. 12, no. 1, pp. 7-14, 2008. [Google Scholar] [Publisher Link]

[5] Dahlia S.A. Al-Jashaami, and Hussein A.M. Al-Zubaidi, "Non-Linear Regression of Air-Water Temperature for Modelling Surface Heat Fluxes in Waterbodies: A Case Study of Laurance Lake, US," *Materials Today: Proceedings*, vol. 80, no. 3, pp. 2631-2637, 2023. [CrossRef] [Google Scholar] [Publisher Link]

[6] S. Anandakumar, T. Subramani, and L. Elango, "Spatial Variation of Groundwater Quality and Inter Elemental Correlation Studies in Lower Bhavani River Basin, Tamil Nadu, India," *Nature Environment and Pollution Technology*, vol. 6, no. 2, pp. 235-239, 2007. [Google Scholar] [Publisher Link]

[7] Biljana Basarin et al., "Trends and Multi-Annual Variability of Water Temperatures in the River Danube, Serbia," *Hydrological Processes*, vol. 30, no. 18, pp. 3315-3329, 2016. [CrossRef] [Google Scholar] [Publisher Link]

[8] Loubna Benyahya et al., "A Review of Statistical Water Temperature Models," *Canadian Water Resources Journal*, vol. 32, no. 3, pp. 179-192, 2007. [CrossRef] [Google Scholar] [Publisher Link]

[9] Bilal Bhat, Saltanat Parveen, and Taskeena Hassan, "Seasonal Assessment of Physicochemical Parameters and Evaluation of Water Quality of River Yamuna, India," *Advances in environmental technology*, vol. 4, no. 1, pp. 41-49, 2018. [CrossRef] [Google Scholar] [Publisher Link]

[10] Joanna R. Blaszczak et al., "Extent, Patterns, and Drivers of Hypoxia in the World's Streams and Rivers," *Limnology and Oceanography Letters*, vol. 8, no. 3, pp. 453-463, 2023. [CrossRef] [Google Scholar] [Publisher Link]

[11] Huayang Cai et al., "Quantifying the Impact of the Three Gorges Dam on the Thermal Dynamics of the Yangtze River," *Environmental Research Letters*, vol. 13, no. 5, pp. 1-14, 2018. [CrossRef] [Google Scholar] [Publisher Link]

[12] Soo Yeon Choi, and Il Won Seo, "Prediction of Fecal Coliform Using Logistic Regression and Tree-Based Classification Models in the North Han River, South Korea," *Journal of Hydro Environment Research*, vol. 21, pp. 96-108, 2018. [CrossRef] [Google Scholar] [Publisher Link]

[13] Gang Chen, and Xing Fang, "Accuracy of Hourly Water Temperatures in Rivers Calculated from Air Temperatures," *Water*, vol. 7, no. 3, pp. 1068-1087, 2015. [CrossRef] [Google Scholar] [Publisher Link]

[14] Daniel Caissie, and Charles H. Luce, "Quantifying Streamed Advection and Conduction Heat Fluxes," *Water Resources Research*, vol. 53, no. 2, pp. 1595-1624, 2017. [CrossRef] [Google Scholar] [Publisher Link]

[15] Javad Daneshi, Amir Naserin, and Saied Jalily, "Determining the Best Discharge-Suspended Sediment Relationship based on Different Time Classifications and Correction Coefficients (Case Study: Bashar River)," *Iranian Journal of Ecohydrology*, vol. 10, no. 1, pp. 113-125, 2023. [CrossRef] [Google Scholar] [Publisher Link]

[16] Marlene Dordoni et al., "Novel Evaluations of Sources and Sinks of Dissolved Oxygen Via Stable Isotopes in Lentic Water Bodies," *Science of The Total Environment*, vol. 838, no. 3, 2022. [CrossRef] [Google Scholar] [Publisher Link]

[17] Benoît O. L. Demars et al., "Impact of Warming on CO_2 Emissions from Streams Countered by Aquatic Photosynthesis," *Nature Geoscience*, vol. 9, pp. 758-761, 2016. [CrossRef] [Google Scholar] [Publisher Link]

[18] Gerd Eiden, "Land-Cover and Land-Use Mapping," *Encyclopedia of Life and Support System–EOLSS: Land Cover, Land Use and Soil Sciences*, vol. 1, pp. 1-9, 2008. [Google Scholar] [Publisher Link]

[19] Golmar Golmohammadi et al., "Predicting the Temporal Variation of Flow Contributing Areas using SWAT," *Journal of Hydrology*, vol. 547, pp. 375-386, 2017. [CrossRef] [Google Scholar] [Publisher Link]

[20] Hoshin Vijai Gupta, Soroosh Sorooshian, and Patrice Ogou Yapo, "Status of Automatic Calibration for Hydrologic Models: Comparison with Multilevel Expert Calibration," *Journal of Hydrologic Engineering*, vol. 4, no. 2, pp. 135-143, 1999. [CrossRef] [Google Scholar] [Publisher Link]

[21] Robert O. Hall et al., "Turbidity, Light, Temperature, and Hydropeaking Control Primary Productivity in the Colorado River, Grand Canyon," *Limnology and Oceanography*, vol. 60, no. 2, pp. 512-526, 2015. [CrossRef] [Google Scholar] [Publisher Link]

[22] Alexander D. Huryn, Jonathan P. Benstead, and Stephanie M. Parker, "Seasonal Changes in Light Availability Modify the Temperature Dependence of Ecosystem Metabolism in an Arctic Stream," *Ecology*, vol. 95, no. 10, pp. 2826-2839, 2014. [CrossRef] [Google Scholar] [Publisher Link]

[23] Douglas Helm, "The Development of the Land Capability Classification," *Readings in the history of the Soil Conservation Service*, pp. 60-73. 1992. [Google Scholar] [Publisher Link]

[24] Sushil Kumar Himanshu et al., "Evaluation of Best Management Practices for Sediment and Nutrient Loss Control Using SWAT Model," *Soil and Tillage Research*, vol. 192, pp. 42-58, 2019. [CrossRef] [Google Scholar] [Publisher Link]

[25] Adam Johnson et al., "Remote Sensing, GIS, and Land Use and Land Cover Mapping along the I-10 Corridor," *International Society for Photogrammetry and Remote Sensing*, pp. 1-9, 2012. [Google Scholar] [Publisher Link]

[26] Margaret M. Kalcic, Indrajeet Chaubey, and Jane Frankenberger, "Defining Soil and Water Assessment Tool (SWAT) Hydrologic Response Units (HRUs) by Field Boundaries," *International Journal of Agricultural and Biological Engineering*, vol. 8, no. 3, pp. 69-80, 2015. [CrossRef] [Google Scholar] [Publisher Link]

[27] Abdulwahd A. Kassem et al., "Predicting of Daily Khazir Basin Flow using SWAT and Hybrid SWAT-ANN Models," *Ain Shams Engineering Journal*, vol. 11, no. 2, pp. 435-443, 2020. [CrossRef] [Google Scholar] [Publisher Link]

[28] David R. Legates, and Gregory J. McCabe, "Evaluating the use of "Goodness-of-Fit" Measures in Hydrologic and Hydroclimatic Model Validation," *Water Resources Research*, vol. 35, no. 1, pp. 233-241, 1999. [CrossRef] [Google Scholar] [Publisher Link]

[29] Xiaobo Luan et al., "Quantitative Study of the Crop Production Water Footprint using the SWAT Model," *Ecological Indicators*, vol. 89, pp. 1-10, 2018. [CrossRef] [Google Scholar] [Publisher Link]

[30] V.S. Malunjkar et al., "Estimation of Surface Runoff using SWAT Model," *International Journal of Inventive Engineering and Sciences*, vol. 3, no. 4, pp. 12-15, 2015. [Google Scholar] [Publisher Link]

[31] Kaleab Habte Michael Mamo, and Manoj K. Jain, "Runoff and Sediment Modeling using SWAT in Gumera Catchment, Ethiopia," *Open Journal of Modern Hydrology*, vol. 3, no. 4, pp. 1-10, 2013. [CrossRef] [Google Scholar] [Publisher Link]

[32] Thanh Son Ngo, Duy Binh Nguyen, and Prasad Shrestha Rajendra, "Effect of Land Use Change on Runoff and Sediment Yield in Da River Basin of Hoah Binh Province, Northwest Vietnam," *Journal of Mountain Science*, vol. 12, pp. 1051-1064, 2015. [CrossRef] [Google Scholar] [Publisher Link]

[33] Navideh Noori, and Latif Kalin, "Coupling SWAT and ANN Models for Enhanced Daily Stream Flow Prediction," *Journal of Hydrology*, vol. 533, pp. 141-151, 2016. [CrossRef] [Google Scholar] [Publisher Link]

[34] G.A. Oluwatosin et al., "From Land Capability Classification to Soil Quality: An Assessment," *Tropical and Subtropical Agroecosystems*, vol. 6, pp. 45-55, 2006. [Google Scholar] [Publisher Link]

[35] Valeriy Osypov et al., "The Desna River Daily Multi-Site Streamflow Modeling using SWAT with Detail Snow Melt Adjustment," *Journal of Geography and Geology*, vol. 10, no. 3, pp. 92-110, 2018. [CrossRef] [Google Scholar] [Publisher Link]

[36] Donizete dos R. Pereira et al., "Hydrological Simulation in a Basin of Typical Tropical Climate and Soil using the SWAT Model Part I: Calibration and Validation Tests," *Journal of Hydrology: Regional Studies*, vol. 7, pp. 14-37, 2016. [CrossRef] [Google Scholar] [Publisher Link]

[37] J.R. Peterson, and J.M. Hamlett, "Hydrological Calibration of the SWAT Model in a Watershed Containing Fragipan Soils," *JAWRA Journal of the American Water Resources Association*, vol. 34, no. 3, pp. 531-544, 1998. [CrossRef] [Google Scholar] [Publisher Link]

[38] Flora Rembert et al., "Interpreting Self-Potential Signal during Reactive Transport: Application to Calcite Dissolution and Precipitation," *Water*, vol. 14, no. 10, pp. 1-31, 2022. [CrossRef] [Google Scholar] [Publisher Link]

[39] M.C. Ramos, C. Benito, and J.A. Martínez-Casasnovas, "Simulating Soil Conservation Measures to Control Soil and Nutrient Losses in a Small, Vineyard Dominated, Basin," *Agriculture, Ecosystems & Environment*, vol. 213, pp. 194-208, 2015. [CrossRef] [Google Scholar] [Publisher Link]

[40] Iwan Ridwansyah et al., "Watershed Modeling with Arc SWAT and SUFI2 in Cisadane Catchment Area: Calibration and Validation of River Flow Prediction," *International Journal of Science and Engineering*, vol. 6, no. 2, pp. 92-101, 2014. [CrossRef] [Google Scholar] [Publisher Link]

[41] S. Sandoval-Solis, D. C. McKinney, and D. P. Loucks, "Sustainability Index for Water Resources Planning and Management," *Journal of Water Resources Planning and Management*, vol. 137, no. 5, pp. 381-390, 2011. [CrossRef] [Google Scholar] [Publisher Link]

[42] Eleni Savvidou, Ourania Tzoraki, Dimitrios Skarlatos, "Delineating Hydrological Response Units in a Mountainous Catchment and its Evaluation on Water Mass Balance and Model Performance," *Second International Conference on Remote Sensing and Geoformation of the Environment International Society for Optics and Photonics*, vol. 9229, 2014. [CrossRef] [Google Scholar] [Publisher Link]

[43] Tejaswini, and K.K. Sathian, "Calibration and Validation of Swat Model for Kunthipuzha Basin using SUFI-2 Algorithm," *International Journal of Current Microbiology and Applied Sciences*, vol. 7, no. 1, pp. 2162-2172, 2018. [CrossRef] [Google Scholar] [Publisher Link]

[44] K.G. Tejwani, "Using and Interpreting Soil Information for Land Capability, Irrigability and Range Site Classification and for Highways," *Soil Conservation Digest*, vol. 4, no. 2, pp. 1-35, 1976. [Google Scholar] [Publisher Link]

[45] Abeyou W. Worqlul et al., "Evaluating Hydrologic Responses to Soil Characteristics using SWAT Model in a Paired-Watersheds in the Upper Blue Nile Basin," *Catena*, vol. 163, pp. 332-341, 2018. [CrossRef] [Google Scholar] [Publisher Link]

[46] Siwei Wang et al., "Water Retention Characteristics and Vegetation Growth of Biopolymer-Treated Silt Soils," *Soil and Tillage Research*, vol. 225, 2023. [CrossRef] [Google Scholar] [Publisher Link]

[47] Wenting Yang, Di Long, and Peng Bai, "Impacts of Future Land Cover and Climate Changes on Runoff in the Mostly Afforested River Basin in North China," *Journal of Hydrology*, vol. 570, pp. 201-219, 2019. [CrossRef] [Google Scholar] [Publisher Link]

Appendix

Table 2. Interpretation of geophysical data

VES No.	VES Location	Resistivity Ohm-m /Thickness m								Curve Types
		Soil Thickness (h_1)	Soil Resistivity (ρ_1)	Weathered Zone Thickness (h_1)	Weathered Zone Resistivity (ρ_1)	First Fracture Zone Thickness (h_1)	First Fracture Zone Resistivity (ρ_1)	Second Fracture Zone Thickness (h_1)	Second Fracture Zone Resistivity (ρ_1)	
1	Karai Elaipalayam	2.3	30.8	35.9	22566.0	9.7	15153.0	72.0	155.0	KQ
2	Perodu	0.85	23.2	8.99	518	7.11	0.148	108	76.1	KH
3	Sircar Peria akraharam	1.9	427	1.58	4361	5.31	154	61.8	217	KH
4	Kurapalayam	1.38	12.9	1.74	397	19.1	4149	80.7	10.9	AK
5	Muthampalayamm	0.573	29.1	5.09	9949	16.9	448	41.8	16141	KH
6	Punjai Lakkapuram	1.95	7.35	17.9	2911	25.1	98609	40.7	7.41	AK
7	Avalpoondurai	0.977	49.6	1.04	10.2	16.4	3130	105	11.1	HK
8	Modakurichi	1.6	58.5	3.49	228	26.7	5991	138	39.4	AK
9	Pasur	2.22	34	19.6	127	30	205	64	755	AA
10	Arasalur	1.16	168	14.9	490	15.1	3277	104	12.1	AK
11	Kagan	1.36	27.3	5.84	9590	65.5	270	48.2	5527	KH
12	Najai Kolanalli	1.02	0.488	4.89	275	20.5	278	62.2	32002	AA
13	Kongudayampalayam	1.74	88.8	14	332	46.2	2260	65.9	595	AK
14	Anjur	0.447	22.2	1.39	1955	72.2	2473	44.2	331	AK
15	Kodumudi	2.91	30.8	2.86	462	10.4	55.7	110	482	KH
16	Kumbilanparappu	1.0	28.0	10.0	112.0	50.0	450.0	80.0	526.0	AA
17	Gangapuram	2.0	180.0	10.0	450.0	28.0	650.0	75.0	560.0	AK
18	Suriyampalayam	2.5	208.0	8.0	375.0	41.0	185.0	51.0	321.0	KH
19	Villarasampatti	2.0	125.0	16.0	708.0	26.0	214.0	31.0	109.0	KQ
20	Vairapalaiyam	1.0	63.0	10.0	158.0	43.0	670.0	62.0	753.0	AA
21	Periyasemur	2.0	83.0	29.0	375.0	34.0	1375.0	57.0	425.0	AK
22	Attayampalaya	2.0	242.0	20.0	859.0	40.0	2362.0	62.0	630.0	AK
23	Veppampalayam	0.5	1671.0	19.6	240.0	32.4	943.0	71.0	146.0	HK
24	Kollampalayam	2.5	45.0	18.5	1100.0	35.0	222.0	65.0	857.0	KH
25	Kanagapuran	1.0	126.0	12.0	220.0	50.0	1848.0	63.0	1575.0	AK
26	sathyamangalam	2.6	119.0	16.0	750.0	21.0	2524.0	50.0	600.0	AK
27	Avalpundurai 2	0.6	339.0	13.8	35.0	37.9	295.0	56.0	500.0	HA
28	Vadugapatti	2.2	119.0	31.0	1187.0	40.0	500.0	55.0	2500.0	KH
29	Attavanai hanumanpalli	1.6	506.0	14.5	233.0	26.9	1248.0	50.4	452.0	HK
30	Peelamedu	0.5	66.0	18.0	375.0	34.0	116.0	50.0	300.0	KH
31	Kangayampalayam	3.0	100.0	16.0	417.0	50.0	2333.0	60.0	261.0	AK
32	Punjai Kalamangalam	4.0	250.0	12.0	500.0	47.0	899.0	76.0	660.0	AK

33	Punduraisemur	1.0	109.0	19.0	308.0	26.0	5750.0	54.0	265.0	AK
34	Sivagiri	2.0	420.0	10.0	630.0	30.0	504.0	60.0	1260.0	KH
35	Injampalli	2.0	175.0	30.0	393.0	38.0	700.0	100.0	930.0	AA
36	Elunoothimangalam	2.7	113.0	20.7	258.0	28.3	4121.0	42.7	640.0	AK
37	Vengampudur	2.0	42.0	10.0	150.0	25.0	350.0	50.0	630.0	AA

Table 3: Pre-monsoon of the physical and chemical parameters of the groundwater

Parameters	Units	Minimum	Maximum	Mean	Median	Standard deviation
pH	-	6.80	8.70	7.63	7.60	0.39
EC	µS/cm	300.00	5880.00	1359.08	1010.00	1003.80
TDS	mg/l	152.00	3362.00	825.06	620.00	588.79
TH	mg/l	41.00	1500.00	382.87	320.00	241.95
Na^+	mg/l	0.00	840.19	125.26	85.10	139.38
K^+	mg/l	1.56	344.08	29.40	18.00	46.25
Ca^{2+}	mg/l	2.20	316.00	71.63	64.00	45.84
Mg^{2+}	mg/l	7.00	196.99	48.07	35.26	37.56
Cl^-	mg/l	17.73	1304.56	175.32	82.00	242.20
HCO_3^-	mg/l	158.60	1360.30	424.46	384.30	170.70
CO_3^{2-}	mg/l	0.00	48.00	3.15	0.00	10.03
SO_4^{2-}	mg/l	2.40	436.80	69.62	47.52	70.20
NO_3^-	mg/l	1.00	181.04	41.32	26.66	38.67
F^-	mg/l	0.10	1.86	0.79	0.66	0.47
Fe	mg/l	0.00	5.10	0.36	0.00	0.87
K. Ratio	meq/l	0.00	3.52	0.74	0.62	0.57
Mg ratio	meq/l	14.61	98.20	51.25	51.11	17.73
RSC	meq/l	-23.37	6.60	-0.47	0.00	3.81
SAR	-	0.00	11.12	2.71	2.04	2.16
% Na	%	2.77	79.71	41.12	41.19	15.49

Table 4: Post-monsoon season of the physical and chemical parameters of the groundwater.

Parameters	Units	Minimum	Maximum	Mean	Median	Standard deviation
pH	-	6.78	8.73	7.78	7.79	0.36
EC	µS/cm	356.00	7098.00	1359.08	1072.00	1110.40
TDS	mg/l	249.00	4968.00	951.35	751.00	777.31
TH	mg/l	112.00	900.00	305.46	280.00	146.06

Na^+	mg/l	15.00	1360.00	137.96	86.00	180.12
K^+	mg/l	3.00	200.00	34.90	23.00	33.69
Ca^{2+}	mg/l	31.00	304.00	77.02	61.00	44.05
Mg^{2+}	mg/l	4.00	84.00	28.40	26.00	16.35
Cl^-	mg/l	20.00	1660.00	176.08	86.00	274.68
HCO_3^-	mg/l	230.00	935.00	526.86	521.00	156.62
CO_3^{2-}	mg/l	0.00	56.00	3.49	0.00	11.17
SO_4^{2-}	mg/l	6.00	763.00	85.56	59.00	99.36
NO_3^-	mg/l	0.00	235.00	28.61	14.00	34.69
F^-	mg/l	0.10	2.00	0.81	0.70	0.43
Fe	mg/l	0.00	6.44	0.40	0.00	1.00
K. Ratio	meq/l	0.18	6.76	0.85	0.64	0.76
Mg ratio	meq/l	7.61	65.61	37.30	38.04	13.30
RSC	meq/l	-9.43	7.76	2.57	2.98	3.07
SAR	-	0.48	28.27	3.12	2.03	3.37
% Na	%	20.84	87.67	45.42	42.22	12.88

Table 6. Inter-element correlation matrix for groundwater samples: Analysis of premonsoon

Parameter	EC	pH	Ca^{2+}	Mg^{2+}	Na^+	K^+	- HCO_3	2- CO_3	2- SO_4	Cl^-	- NO_3	F	TDS	TH	Tur	Palk	Talk	Fe	NH_3	NO_2	PO_4
EC	1																				
pH	-0.245	1																			
Ca^{2+}	0.722	-0.347	1																		
Mg^{2+}	0.758	-0.025	0.538	1																	
Na^+	0.361	-0.061	0.209	0.266	1																
K^+	0.254	0.061	0.102	0.278	0.009	1															
-HCO_3	0.693	-0.181	0.345	0.649	0.315	0.228	1														
2-CO_3	-0.079	0.512	-0.136	0.02	-0.077	0.053	-0.194	1													
2-SO_4	0.661	-0.102	0.398	0.497	0.229	0.204	0.392	0.016	1												
Cl^-	0.963	-0.253	0.76	0.704	0.345	0.216	0.557	-0.071	0.561	1											
-NO_3	0.502	-0.176	0.534	0.361	0.094	0.224	0.231	-0.117	0.258	0.459	1										
F^-	0.415	0.018	0.142	0.371	0.162	-0.005	0.493	-0.125	0.291	0.331	0.159	1									
TDS	0.976	-0.299	0.72	0.705	0.347	0.3	0.652	-0.096	0.725	0.946	0.477	0.37	1								
TH	0.841	-0.23	0.822	0.875	0.267	0.223	0.592	-0.058	0.528	0.833	0.517	0.339	0.818	1							

Tur	0.21	-0.312	0.13	0.149	0.1	-0.025	0.369	-0.095	0.014	0.17	0.067	0.003	0.216	0.171	1						
Palk	-0.015	0.094	-0.053	-0.019	-0.015	0.186	0.026	0.035	-0.054	-0.022	-0.016	0.065	-0.011	-0.042	-0.055	1					
Talk	0.36	-0.086	0.153	0.242	0.193	0.113	0.402	-0.178	0.318	0.271	0.115	0.392	0.384	0.25	0.173	-0.009	1				
Fe	0.158	-0.308	0.085	0.121	0.065	-0.039	0.298	-0.087	-0.015	0.125	0.097	-0.015	0.161	0.128	0.926	-0.051	0.115	1			
NH_3	0.086	-0.039	0.027	0.065	0.016	-0.01	0.066	-0.014	0.112	0.064	0.095	-0.012	0.079	0.052	0.06	-0.046	0.01	0.045	1		
NO_2	0.205	-0.077	0.08	0.025	0.049	0.051	0.271	-0.08	0.081	0.138	0.179	0.283	0.189	0.172	0.194	-0.041	0.442	0.082	0.037	1	
PO_4	0.127	-0.071	0.18	0.13	-0.024	0.058	0.08	0.101	0.115	0.095	0.271	-0.01	0.16	0.196	0.348	-0.097	0.338	0.377	0.026	0.159	1

Table 7. Matrix of inter-element correlation for groundwater samples, Analysis of postmonsoon

Parameter	Tur	EC	TDS	pH	Palk	Talk	TH	Ca^{2+}	Mg^{2+}	Na^{+}	K^{+}	Fe	NH3	NO2	$-NO_3$	CL^{-}	F^{-}	SO4	PO4	$-HCO_3$	$2-CO_3$
Tur	1																				
EC	0.072	1																			
TDS	0.072	1	1																		
pH	-0.392	-0.178	-0.178	1																	
Palk	-0.058	-0.05	-0.05	0.31	1																
Talk	0.147	0.477	0.477	-0.272	-0.008	1															
TH	0.197	0.793	0.793	-0.389	-0.113	0.578	1														
Ca^{2+}	0.135	0.846	0.846	-0.271	-0.099	0.457	0.878	1													
Mg^{2+}	0.191	0.372	0.373	-0.369	-0.087	0.627	0.662	0.297	1												
Na^{+}	0.011	0.964	0.964	-0.072	-0.018	0.326	0.634	0.716	0.218	1											
K^{+}	0.098	0.76	0.76	-0.16	-0.082	0.57	0.587	0.676	0.276	0.674	1										
Fe	0.922	0.063	0.063	-0.344	-0.051	0.152	0.174	0.127	0.157	0.006	0.121	1									
NH_3	0.133	0.121	0.121	-0.046	-0.045	0.148	0.005	0.099	0.159	0.087	0.234	0.119	1								
NO_2	0.169	0.212	0.212	-0.104	-0.04	0.429	0.22	0.152	0.392	0.143	0.262	0.122	0.405	1							
$-NO_3$	0.353	0.326	0.326	-0.377	-0.1	0.364	0.455	0.391	0.313	0.213	0.351	0.384	-0.002	0.161	1						
CL^{-}	0.027	0.976	0.976	-0.125	-0.048	0.315	0.749	0.847	0.255	0.959	0.692	0.011	0.105	0.144	0.229	1					
F^{-}	-0.028	0.366	0.366	0.009	0.084	0.544	0.321	0.213	0.364	0.333	0.297	0.013	0.086	0.234	0.191	0.27	1				
SO_4	0.075	0.906	0.906	-0.09	-0.056	0.322	0.633	0.652	0.335	0.926	0.62	0.067	0.081	0.133	0.239	0.866	0.328	1			
PO_4	-0.068	0.23	0.231	0.06	0.005	-0.095	0.11	0.189	-0.039	0.272	0.038	-0.055	0.179	-0.011	-0.051	0.286	0.123	0.221	1		
$-HCO_3$	0.097	0.5	0.5	-0.255	0	0.791	0.477	0.395	0.486	0.43	0.568	0.112	0.204	0.402	0.161	0.356	0.475	0.409	-0.115	1	
$2-CO_3$	-0.106	-0.025	-0.025	0.208	0.04	-0.157	-0.111	-0.043	-0.181	0.022	-0.115	-0.094	-0.013	-0.079	0.087	0.012	-0.08	-0.016	0.259	-0.358	1